Effects of Fuel Reactivity and Injection Timing on Diesel Engine Combustion and Emissions

S. K. Aggarwal, X. Fu, and S. Wijeyakulasuriya[1]
University of Illinois at Chicago, Chicago, IL, USA
[1]Convergent Science, Middleton, WI, USA

Corresponding Author: Suresh K. Aggarwal
University of Illinois at Chicago,
842 W, Taylor St, Chicago, IL 60607, USA
Phone: 312-996-2235
Fax: 312-413-0447
Email: ska@uic.edu

Revised: April 28, 2014

Keywords: Diesel engine, fuel reactivity, ignition delay, premixed combustion, NOx and soot emission.

ABSTRACT

Recent strategies for simultaneously reducing NOx and soot emissions have focused on achieving nearly premixed, low-temperature combustion in diesel engines. A promising approach in this regard is to vary fuel reactivity in order to control the ignition delay and optimize the level of premixing and reduce emissions. The present study examines such a strategy by performing 3-D simulations in a single-cylinder of a diesel engine. Simulations employ the state-of-the-art two-phase models and a validated semi-detailed reaction mechanism. The fuel reactivity is varied by using a blend of n-heptane and iso-octane, which represent surrogates for gasoline and diesel fuels, respectively. Results indicate that the fuel reactivity strongly influences ignition delay and combustion phasing, whereas the start of injection (SOI) affects combustion phasing. As fuel reactivity is reduced, the ignition delay is increased and the combustion phasing is retarded. The longer ignition delay provides additional time for mixing, and reduces equivalence ratio stratification. Consequently, the premixed combustion is enhanced relative to diffusion combustion, and thus the soot emission is reduced. NOx emission is also reduced due to reduced diffusion combustion and lower peak temperatures caused by delayed combustion phasing. An operability range is observed in terms of fuel reactivity and SOI, beyond which the mixture may not be sufficiently well mixed, or compression ignited. The study demonstrates the possibility of finding an optimum range of fuel reactivity, SOI, and EGR for significantly reducing engine out emissions for a given load and speed.

***Keywords**: Diesel engine, fuel reactivity, ignition delay, premixed combustion, NOx and soot emission.*

Introduction

Increasingly strict emission standards in the U.S. and Europe are providing a major impetus to engine manufacturers for developing advanced engine technologies. A conventional diesel engine employs fuel injection near the top dead center (TDC), a relatively short time for fuel-air mixing and ignition, and high-temperature combustion occurring over a wide range of equivalence ratios. While it offers significant advantage in terms of durability and efficiency, an expensive after-treatment is required to meet emission regulations for NOx, particulate matter (PM) and other pollutants. Moreover, most strategies used to reduce exhaust emissions exhibit the well-known soot-NOx tradeoff behavior. In this context, recent studies have focused on achieving pre-mixed, low-temperature combustion (LTC) in order to reduce emissions without any detrimental effect on fuel consumption and energy density. Different strategies that have been investigated include homogeneously charged compression ignition

(HCCI) (Tanaka et al. 2003, Kong and Reitz 2002, Dec 2009, and Mueller et al. 2004), modulated kinetics (MK) concept (Kimura et al. 2001), premixed charge compression ignition (PCCI) (Diwakar and Singh 2008), and reactivity controlled compression ignition (RCCI) (Reitz 2012). While there are some differences in these strategies, the underlying concept is to avoid high-temperature and fuel rich (high equivalence ratio (ϕ)) regions. Lowering flame temperatures results in reduced NOx formation, while increasing the amount of premixed combustion (i.e., lowering ϕ) decreases soot formation. Other measures in this regard include using exhaust gas recirculation (EGR) to reduce flame temperatures, delaying the auto-ignition event by controlling injection parameters and tailoring the fuel reactivity, and reducing fuel-rich zone through enhanced fuel-air mixing (Wang et al. 2007, Ni and Wang 2012, and Brijesh and Chowdhury 2014). *In addition, researchers are examining dual-fuel strategies to reduce emissions without affecting the engine performance (Korakianitis et al. 2011). Such strategies may include directly injecting a pilot fuel (i.e. diesel) with good auto-ignition characteristics, while a gaseous fuel, such as natural gas, is mixed with air and introduced through the intake valve.*

The HCCI concept is based on providing a lean, premixed fuel/air mixture during the compression stroke. The mixture is auto-ignited near the top dead center (TDC), followed by a rapid combustion phase with most of the heat release occurring in 10-35° crank angle (CA). The HCCI engine can exploit the advantages of both the direct injection compression ignition (DICI) and spark ignition (SI) engines, while eliminating their disadvantages. For instance, it eliminates SI knock associated with autoignition of fuel-air mixture in the end zone, and also provides CI type efficiencies due to higher compression ratios and the absence of part-load throttling losses associated with SI engines. Moreover, it can provide significant reduction in both particulates and NOx due to the homogeneous lean burn operation leading to lower gas temperatures and elimination of the fuel rich zones. Lower gas temperatures also reduce losses associated with irreversibilities and heat transfer to walls. While the HCCI operation is quite promising, it has many challenges stemming from the lack of control of the ignition event and combustion phasing, which is defined in terms of the crank angle corresponding to 50% of the total heat release (CA50). In HCCI engines, the ignition timing is not controlled by the fuel injection process as in a DICI engine, or by the spark as in an SI engine. Instead, it is controlled by the temperature, pressure, and composition of the fuel-air mixture. The rate of heat release is also not controlled neither by the rate of fuel injection as in a DICI engine, nor by finite turbulent flame propagation as in an SI engine. As a result, the near constant volume

combustion event leads to a very rapid rate of heat release, thus promoting high mechanical stresses, unacceptable noise, and knock (Gary and Ryan 1999). Thus, there are many unresolved issues with HCCI operation, including the control of ignition timing and combustion phasing over a range of conditions, operation at high loads, increased hydrocarbon (HC) and carbon monoxide (CO) emissions, and difficulty with cold start.

Several strategies have been explored to address the aforementioned challenges. Some have focused on developing active sensor and control strategies to vary the amount of EGR (Kimura et al. 2001), compression ratio (CR) (Christensen et al. 1999), and/or valve timing (Kaahaaina et al. 2001). Others have considered partially stratifying the fuel-air mixture (Lee and Lee 2007) or switching to traditional CIDI combustion at high loads (Reitz 2012). In particular, a practical strategy may employ dual mode combustion, with HCCI at low to medium loads and conventional combustion at high loads. Other LTC strategies are based on using excessive amount of EGR to reduce gas temperatures and achieving nearly premixed combustion through enhanced mixing and shorter injection duration. Kimura et al. (2001) examined such a strategy, termed as the MK concept, by conducting experiments on a 4-cylinder DI engine, and observed that by reducing O_2 concentration from 21% to 15% through EGR, NOx emissions were substantially reduced. However, this led to an increase in UHC and smoke levels, which may be reduced through early injection (SOI) and high swirl.

Another promising approach to have control on ignition and combustion phasing is to vary the fuel reactivity (Reitz 2012, Kalghatgi et al. 2006, Kalghatgi et al 2011) by using a less reactive fuel, such as gasoline, with high resistance to auto-ignition. Such an approach allows the injection process to be completed and more mixing time prior to the start of combustion, producing lower local ϕ and thus lower NOx and soot emissions. The fuel reactivity can also be controlled by employing a dual-fuel strategy, i.e., by using low cetane number (CN) fuel such as gasoline at high loads, and high CN fuel such as diesel at low loads. Reitz (2012) demonstrated a successful implementation of dual fuel strategy, termed as RCCI, by using port fuel injection of less reactive fuel, coupled with optimized in-cylinder multiple injections of more reactive fuel. This strategy was shown to provide sufficient time for fuel vaporization and mixing, as well as equivalence ratio and reactivity stratifications in the chamber. Consequently, the RCCI operation resulted in significant reduction in NOx and PM emissions and extended the engine's operable load range beyond that of HCCI or PCCI.

A similar approach but without using port fuel injection is to vary the fuel reactivity by directly injecting a diesel-gasoline mixture into the cylinder. Then the ignition timing can be controlled by varying the amount of less (or more) reactive fuel in the blend, while the combustion phasing may be controlled by varying injection timing as in a conventional CI engine. Thus, as discussed by Kalghatgi et al. (2006 and 2011) the fuel and air are premixed enough to reduce PM emissions but not fully premixed as in HCCI engines so that in-cycle control over combustion phasing is regained. Also, while the combustion process is still strongly influenced by chemical kinetics, the mixing and transport become relevant. Moreover, the NOx and HC levels can be reduced by using EGR, and by optimizing injection and other parameters. Consequently, a diesel engine can be run at a much higher load compared to that using diesel fuels. This offers the potential for developing engines with high efficiency and low emissions at lower cost and complexity compared to other approaches.

The present study is motivated by these considerations, and examines the potential of simultaneously reducing NOx and soot by controlling the fuel reactivity and injection parameters. The fuel reactivity is varied by using appropriate blends of n-heptane and iso-octane fuels, which are considered good surrogates for diesel and gasoline, respectively. A state-of-the-art 3D CFD methodology is employed to characterize the effects of blend composition and injection timing on the spray behavior, ignition, flame structure, and emissions in a single-cylinder of a light-duty diesel engine.

There has been extensive research dealing with the use of different fuel blends in CI and SI engines. A number of investigations have examined the combustion and emission characteristics of SI engines fueled with gasoline/hydrogen (Changwei and Shuofeng 2009), gasoline/ethanol (Bayraktar 2005) and gasoline/butanol (Irimescu 2012) blends. Similarly numerous studies have focused on using diesel/hydrogen (Saravanan et al. 2008), diesel/butanol (Karabektas and Hosoz 2009), and diesel/biodiesel blends (Lapuerta et al. 2008, Alam et al 2004). The use of n-heptane/iso-octane (Peng et al. 2003, Dumitrescu et al. 2011, Lu et al. 2005, Shahbakhti and Koch 2008, Hu and Cracknell 2011), gasoline/diesel (Kokjohn and Reitz 2009) blends in HCCI, constant volume combustor, and conventional diesel engine has also been investigated. Dumitrescu et al. (2011) performed experiments using a single-cylinder engine fueled with n-heptane/iso-octane mixtures, and observed that the addition of iso-octane reduced combustion efficiency, retarded combustion phasing, and narrowed the range of CR for satisfactory HCCI operation. Furthermore, NOx was found to increase at advanced combustion phasing (CA50) but the effect of iso-octane addition was negligible for

CA50 close to or after TDC. Lu et al. (2005) also performed HCCI engine experiments, and observed that the effect of iso-octane addition was to retard the start of ignition, decrease the peak heat release rate, and increase CO and HC emissions.

In summary, the above literature review indicates that while the use of fuel blends in different engine configurations has been extensively investigated, few studies have examined the effects of using diesel/gasoline or n-heptane/iso-octane blends on engine performance and emissions. Kalghatgi et al. (2011) performed diesel engine experiments with different model fuels–mixtures of iso-octane, n-heptane and toluene–and gasolines of different octane numbers. The fuel reactivity was characterized in terms of an Octane Index (OI), which describes the autoignition quality. These experiments demonstrated the potential of running conventional diesel engines with gasoline like fuels, and a blend of iso-octane/n-heptane/toluene was found to be a good surrogate for gasoline. In addition, the ignition delay and charge stratification were found to be related to OI, although the combustion phasing was less correlated with this parameter. López et al. (2013) reported a numerical study, based on an open-source CFD package (OpenFOAM), to investigate the effect of fuel reactivity on ignition and flame structure in an, axisymmetric, constant volume combustor. Although the results were preliminary, the study demonstrated the capability of CFD-based tools for examining the potential of reducing emissions by varying fuel reactivity.

We report herein a numerical investigation on the effects of fuel reactivity (i.e., Cetane Number (CN)) and injection timing on the performance and emissions of a light-duty diesel engine. A reduced kinetic model for the oxidation of n-heptane/iso-octane blends is developed and extensively validated for engine relevant conditions. The model is implemented in the commercial code, CONVERGE (Richards et al. 2012) for engine simulations, in order to characterize the effects of blend composition and injection timing on the spray, ignition, flame structure, and emissions in a single cylinder of the diesel engine. Other conditions including engine speed, load, EGR, etc., are maintained constant.

The Physical-Numerical Model

The physical-numerical models used in the CONVERGE software have been described in *detail elsewhere (Richards et al. 2012, Som and Aggarwal 2010, Aggarwal and Longman 2011).* Therefore, only a brief summary is presented here. The computational model is based on an Eulerian-Lagrangian description of the two-phase turbulent reacting flow inside the cylinder. The gas-phase flow field is described using the Favre-Averaged Navier-Stokes

equations along with the RNG k-ε turbulence model, which includes source terms to account for the effects of discrete phase on gas-phase turbulence. A finite volume methodology based on a semi-implicit hybrid scheme is used to solve the gas-phase equations on an Eulerian grid. The length and time scales associated with the spray processes are too small to be resolved computationally, necessitating the use of sub-grid scale models to describe the spray physics. The spray is represented by a stochastic system of a discrete number of parcels, which are tracked computationally using a Lagrangian scheme. The two phases are coupled through the mass, momentum, and energy exchange terms, which are present in both the liquid- and gas-phase equations. Liquid-gas coupling is performed using the nearest node approach.

Spray processes that are modeled include fuel atomization, droplet distortion, droplet drag, turbulent dispersion, droplet interactions in terms of collision and coalescence, vaporization, and spray-wall interaction. The injection process is simulated using a blob injection model, which injects liquid droplet parcels with a diameter equal to an effective nozzle diameter. The subsequent breakup process is simulated by using models based on the Kelvin- Helmholtz (KH) and Rayleigh-Taylor (RT) instabilities (Reitz and Diwakar 1987, Patterson and Reitz 1998). The KH instability is due to high shear at the liquid-gas interface, while the RT instability is related to density difference between the two fluids. The droplet breakup occurs by the competing effects of the KH and RT models. The (KH) model considers breakup resulting from unstable waves growing at the liquid surface. The breakup of droplet parcels is calculated by assuming that the radius of newly formed droplets is proportional to the wavelength of the fastest growing unstable surface wave on the parent droplet. The RT model employs a similar approach, by calculating the characteristic length and time scales associated with the RT instability. The KH–RT atomization model has been widely employed for diesel engine simulations, and found to be computationally efficient and reproduce the global spray behavior reasonably well.

Droplet collisions are based on the NTC (No Time Counter) algorithm (Schmidt and Rutland 2000). Once collision occurs, the outcomes of the collision are predicted as bouncing stretching, reflexive separation, or coalescence (Poster and Abraham 2002). A multi-component droplet evaporation model based on the Nusselt number and Sherwood number correlations of Chiang et al. (1992) is used. A dynamic drag model is used which accounts for the effects of drop distortion, linearly varying between the drag of a sphere and a disk (Liu et al. 1993). The oxidation of n-heptane/iso-octane blends is modeled by a validated reduced mechanism, which is implemented in the CFD solver through the SAGE chemical kinetic

solver (Richards et al. 2012, Senecal et al. 2003). Details of the reactions mechanism are provided in a subsequent section.

The CFD solver uses an innovative modified cut-cell Cartesian method for grid generation (Senecal et al. 2003). The computational mesh is generated internally to the code at runtime. Velocities at moving boundaries are user specified and the mesh is redrawn at every time step according to the boundary definitions. Moreover, the adaptive mesh resolution (AMR) technique enables local mesh refinement in regions of high curvatures (2^{nd} derivative of flow variables). For the results presented here, the base (largest) grid size was fixed at 2mm. In order to resolve the flow near the injector, a local refinement area with 0.5mm grid sizes were used, along with 0.5 mm cells for AMR based on the curvature in the velocity, temperature, and species fields. The grid-independence of simulations using these grid parameters is discussed in a later section.

Development and Validation of Reaction Mechanism for n-Heptane/Iso-Octane Blend

A reduced reaction mechanism was developed for the oxidation of n-heptane/iso-octane blends under engine relevant conditions. The Chalmers mechanism (Valeri Golovichev's Home Page) involving 42 species and 168 reactions for n-heptane oxidation was combined with an iso-octane mechanism (Jia and Xie 2006) containing 38 species and 69 reactions. These two mechanisms have previously been validated separately against various targets, including ignition delay and laminar flame speed data, for n-heptane/air and iso-octane/air mixtures, respectively.

The combined mechanism contained 10 common/duplicate reactions with different rate constants. In order to identify the appropriate rate coefficients to be used for these reactions, a sensitivity analysis was performed by varying the reaction rate constants of each of these 20 reactions, and comparing the predicted ignition delays with the shock tube data. Simulations were performed using the closed homogeneous reactor model in CHEMKIN-10101 (Reaction Desion 2010) software for n-heptane/air, iso-octane/air, and n-heptane/iso-octane/air mixtures at engine relevant conditions. The comparison indicated that the ignition delay predictions are mostly sensitive to reaction $H_2O_2+m \Leftrightarrow OH+OH+m$ (R1) involving the decomposition of hydrogen peroxide. Figures 1 and 2 present the effect of R1 rate constants on the predicted ignition delays for n-heptane/air and iso-octane/air mixtures at a pressure (p) of 55 atm and an equivalence ratio (ϕ) of 1. *In these figures, ignition delay (t) is plotted versus the inverse of temperature (T)*, and k1 and k2 represent the rate constants of reaction R1 used in the n-

heptane and iso-octane mechanisms, respectively. Figure 1 compares the predictions with the shock tube measurements of Gauthier et al. (2004) for n-heptane/air mixtures, and with measurements of Davidson et al. (2005) for iso-octane/air mixtures at p=55 atm and ϕ=1. Predictions using the detailed LLNL (Lawrence Livermore National Laboratory) mechanism (LLNL 2013) for iso-octane/air mixtures are also shown in Fig. 1b. Overall there is good agreement between the predictions and measurements for both mixtures. In addition, while the predicted ignition delays are fairly insensitive to the different R1 rate constants for n-heptane/air mixtures, there is greater sensitivity to these constants for iso-octane/air mixtures. For the latter, predictions using the rate constants of iso-octane mechanism (k2) exhibit better agreement with the shock tube data of Davidson (2005).

Figure 2 shows the comparison of predicted ignition delays for the two blends with 60% and 80% iso-octane by volume, and at p=40 atm and ϕ=1, with the measurements of Fieweger et al. (1997). Results for these blends also indicate that the R1 rate constants of iso-octane mechanism (k2) provide closer agreement with the ignition data. Therefore, the R1 rate constants from iso-octane mechanism (k2) were employed in the combined mechanism for the fuel blend. Results of sensitivity study (not shown here) also indicated that the kinetic parameters of reactions R2-R10 have no noticeable effect on the predicted ignition delay for various fuel blends. Consequently, for these reactions, the kinetic parameters of the n-heptane mechanism were used in the combined mechanism, which consisted of 54 species and 190 reactions for n-heptane/iso-octane combustion and NOx formation. Rate constants for reactions R1-R10 are provided in Table 1. Results of another validation for the combined mechanism are presented in Fig. 3, which plots the predicted ignition delay times for three different blends containing 0, 10%, 50%, and 90% iso-octane by volume. Predictions using the detailed LLNL mechanism for 50%-, and 90%-iso-octane blends are also shown in this figure. There is fairly good agreement between the predictions of the two mechanisms, although the combined mechanism underpredicts the ignition delay times compared to the LLNL mechanism at temperatures below 1000K. Moreover, for both mechanisms, the ignition delay time increases noticeably as the amount of iso-octane in the blend is increased. This has important consequences with regards to the effect of fuel Cetane number (or reactivity) on diesel combustion and emissions, as discussed in the next section. It is also important to note that the combined mechanism is able to capture the NTC (negative temperature coefficient) regime quite well. The mechanism is provided as supplementary material with this paper.

Also, as stated earlier, the mechanism was directly coupled with the gas phase calculations through the combustor solver (Richards et al. 2012).

Results and Discussion

The computational model used in the CONVERGE software has been extensively validated in previous studies (Som and Aggarwal 2010, Aggarwal and Longman 2011). For nonevaporating and evaporating sprays, the model was shown to reproduce reasonably well the measured liquid penetration and spray distribution for various conditions. For reacting sprays, validation included matching the flame images, flame liftoff, and liquid lengths with the measurements of Siebers and Higgins (2001) and Higgins and Siebers (2001) in a constant volume combustor under diesel engine conditions (Som and Aggarwal 2010). In addition, the diesel engine simulations have been validated (Aggarwal and Longman 2011) through the comparison of pressure and heat release rate measurements performed at Argonne National Laboratory for the same engine as that used in the present study. Finally, the combined reaction mechanism used in this work has been validated against the ignition delay data as discussed earlier.

For the present study, simulations considered 51.43° sector of a cylinder corresponding to the 1.9L 4-cylinder GM light-duty diesel engine with a 7-hole common-rail injector with only one nozzle hole modeled. The computational domain indicating the 1/7 sector used in simulations is shown in Figure 4. No-slip wall boundary conditions are specified at the piston and cylinder walls including the head, with periodic boundary conditions at the front and back face of the sector. In addition, the law-of-the-wall conditions are specified along with the boundary temperatures. Other conditions used in simulations are provided in Table 2. The start of injection (SOI) and injection duration were determined from the injector-current plot. The peak injection pressure is 22 MPa and the discharge coefficient selected is 0.85. For the present results, injection duration of 8 CAD (crank angle degree) corresponding to part load conditions was used. For such conditions, a triangular rate of injection (ROI) profile has generally been found to simulate the injection process well. The mass of fuel injected taken from one of the experimental conditions is 0.125mg (Aggarwal and Longman 2011).

The grid independence of results was established by performing simulations using different maximum and minimum grid sizes, for both selective refinement and AMR. Some representative results for three different grids are presented in Figure 5, which plots the pressure and chemical heat release rate (HRR) profiles with respect to CAD for n-heptane fuel.

The grid sizes used in fixed refinements and AMR for the three grids are listed in Table 3. As indicated in this table, the largest grid size between times -145 CAD to -22 CAD ATDC was 2mm.

The largest grid size was changed to 1mm after -22 ATDC and used 0.25 mm cells near the injection nozzle, and 0.5mm cells near the piston wall and cylinder head to resolve near wall flow (Standard wall function is turned ON). With AMR, 0.25 mm cells are *used to resolve regions with large velocity, temperature, and species gradients*. As indicated in Figure 5, results are nearly the same for Cases 1 and 2. Consequently, grid setting of Case 2 with the minimum grid size of 0.5 mm was used for most of simulations. In the following, we present results examining the effects of fuel reactivity and injection timing on the combustion and emission characteristics.

Effect of Fuel Reactivity on Combustion and Emissions

The fuel reactivity was varied by considering three n-heptane/iso-octane blends containing 0%, 10%, and 50% iso-octane by volume. As noted in the literature, Cetane Numbers (CN) of the two fuels are approximately 56 and 16, with the corresponding Octane Numbers of 0 and 100, respectively. The start of injection (SOI) for these simulations was specified as -8°CA ATDC. Figure 6 presents average cylinder pressure and heat release rate (HRR) profiles with respect to CAD for the three blends. As expected, the addition of iso-octane has a significant effect on the ignition and combustion processes. As the amount of iso-octane in the blend is increased, the total ignition delay time (t_{ig}), defined as the interval between the end of injection and the start of self-sustained combustion as indicated in the HRR profiles, increases from 8 CAD for 0%-iso-octane to 9.5 CAD for 10%-iso-octane, and 11 CAD for 50%-iso-octane blend. In addition, for the 90%-iso-octane blend, the mixture fails to ignite, i.e., the ignition delay time is too large and the piston goes into the expansion stroke during which the pressure and temperature decrease. Values of ignition delays and other computed properties are provided in Table 4.

As discussed in Aggarwal and Longman (2011) and Aggarwal (1998), the ignition delay time may be divided into a physical delay (t_p), associated with the atomization, vaporization and mixing processes, and a chemical delay (t_c) during which the radical activity and heat release rates become significant and the combustion becomes self-sustaining. As inferred from the

HRR profiles, the physical delay[1] is essentially the same for the three blends, its value being 5° CA, implying that the spray atomization and vaporization processes are not noticeably affected by fuel reactivity. However, the ignition and combustion processes are strongly influenced by the blend composition. The chemical delays for the three blends are 3°, 5°, and 6°CA, respectively. As a consequence, the combustion phasing, defined in terms of the crank angle corresponding to 50% heat release (CA50), increases with the amount of iso-octane in the blend; its values are 2°CA, 5°CA, and 6°CA ATDC, respectively, for the three blends. Thus the ignition delay and combustion phasing are well correlated with the fuel reactivity. Furthermore, the total heat release, computed from the HRR plots, decreases with the addition of iso-octane, its values being 381J, 377J, and 370J for the three blends. This can be attributed to the lower heating value and reactively of iso-octane compared to n-heptane. The lower reactivity of iso-octane leads to incomplete combustion and results in higher UHC. Some important properties of n-heptane and iso-octane fuels are listed in Table 5.

The effect of fuel reactivity on engine performance can be characterized in terms of total work output, mean effective pressure (MEP), and power. As indicated in Table 6, the work output values, corresponding to the included area of each pressure-volume curve, were 166J, 161J, and 151J for the three blends. The corresponding values of MEP were 2445.5 kPa, 2372.3 kPa, and 2224.7kPa, while those of power were 14.6 kW, 14.2 kW, and 13.3 kW. Thus, the power output slightly decreases with iso-octane addition, which again may be due to lower reactivity of the blend, leading to some incomplete combustion and higher UHC formation. For instance, the total UHC mass at EVO in the cylinder were estimated to be $1.6*10^{-7}$, $2.0*10^{-7}$, $3.3*10^{-7}$ kg for the three fuel blends, respectively. The mass of all chemical species which have H and C atoms in them constitute the UHC emissions.

The effect of fuel reactivity on overall emissions is illustrated in Fig. 7, which plots the amounts of NOx and soot formed versus crank angle for the three blends. As discussed in by Richards et al. (2012), the NOx and soot formation models are based on the extended Zeldovich mechanism and Hiroyasu and Kadota's model, respectively. In the soot model, the sum of all unburnt hydrocarbon species is used as the soot formation species. Results indicate that both NOx and soot emissions are in general significantly reduced as the fuel reactivity is reduced. The normalized emissions (g/kW·h) based on engine power (cf. Table 6) are also considerably reduced, especially for the 50-50 blend. The NOx reduction may be related to

[1]Both the physical delay and chemical delay are marked in the HRR plots in Fig. 6.

lower combustion temperatures, which can be attributed to the fact that lower fuel reactivity retards combustion phasing, and, consequently, combustion occurs further into the expansion stroke when the cylinder temperature and pressure are lower. *As mentioned earlier, the combustion phasing (CA50) increases from 2° for the 0%-iso-octane case to 5° ATDC for 10%-iso-octane case. The reduction in soot emission is related to the increased level of premixing as a result of longer ignition delay caused by iso-octane addition.* This aspect is further discussed below.

Further insight into the effect of fuel reactivity on the spray combustion and emission processes can be gained by analyzing spray distribution and temperature contours, shown in Figures 8 and 9, for the 0%- and 50%-iso-octane blends. The spray distribution is plotted in terms of the instantaneous droplet locations at crank angles corresponding to the fuel injection and spray development prior to ignition, while temperature contours are shown at crank angles that best depict the ignition and combustion processes. The spray injection and vaporization processes appear to be quite similar for the two blends, which is consistent with the earlier observation that the physical delay times are the same for these blends. In contrast, the ignition and combustion processes are significantly influenced by fuel reactivity. As indicated by temperature contours, ignition occurs near 0° ATDC for the 0% iso-octane case, and near 3° ATDC for the 50% iso-octane case. The longer ignition delay provides additional time for fuel-air mixing, and, thus, more premixed combustion for the latter case. This can be seen by comparing the temperature contours at 4° and 8° ATDC for the 0%- and 50%-iso-octane cases, respectively. Moreover, a broader HRR profile with lower peak (cf. Fig. 6) provides further evidence of enhanced premixed combustion for the 50%-iso-octane case. As a consequence, the NOx and soot emissions are strongly modified by fuel reactivity, as indicated in Fig. 10, which plots the temperature, equivalence ratio (ϕ), NOx, and soot contours at 4° ATDC for the 0% iso-octane case, and at 7° ATDC for the 50% iso-octane case. Note that different crank angles used in these plots account for the difference in combustion phasing for the two cases.

Several important observations can be made from Fig. 10. First, as a consequence of the piston bowl geometry, the fuel consumption and heat release occur in two separate regions, one in piston bowl and other in the spray region between the piston and cylinder walls. The temperature and equivalence ratio (ϕ) contours indicate that combustion in the piston bowl region involves both the rich premixed and diffusion burning zones, while that in the cylinder region involves lean premixed burning. Second, while there are distinct zones of rich

premixed and diffusion burning, the combustion process does not follow the conventional Dec's model (Som and Aggarwal 2010, Flynn et al. 1999), which is characterized by a lifted flame with rich premixed burning enveloped by diffusion burning. Third, the amount of NOx and soot produced is mostly determined by the relative amounts of rich premixed and diffusion burning, local temperatures, and the presence of wall. The contour plots in Fig. 10 clearly indicate that the soot formation region corresponds to the rich premixed combustion region, while the NOx is mostly formed in the diffusion combustion region, with the amount of NOx formed strongly influenced by local temperatures. Finally, the longer ignition delay for the 50%-iso-octane case leads to enhanced mixing, which can be discerned from ϕ contours. As indicated, ϕ values in the fuel-rich region range between 1.8-2.8 for the 0%-iso-octane case, and between 1.4-2.2 for the 50%-iso-octane case. As a consequence, the amount of soot produced is significantly reduced for the latter case, which is quite evident from soot contours in Fig. 10. The amount of NOx produced is also reduced due to lower fuel reactivity, and this can be attributed to two factors. One, the amount of diffusion burning is reduced relative to rich premixed burning, and two, the peak temperatures are reduced from ≈2785K for the 0%- iso-octane case to ≈2734K for the 50%-iso-octane case.

Effect of Injection Timing on Engine Combustion and Emissions

Simulations were performed with three SOIs of -15°, -8°, and -0.5°CA ATDC for the 50%-iso-octane blend. Other conditions including the injection duration were the same as listed in Table 2. Figure 11 presents the pressure and HRR profiles for the three SOI cases. The corresponding results for n-heptane (0% iso-octane) have been reported in a previous study (Aggarwal and Longman 2011). As indicated in Fig. 11, for the 0.5° SOI case, the mixture fails to ignite due to lower fuel reactivity and the fact that injection and spray processes occur during the expansion stroke. The total ignition delay times (t_{ig}) for the -15° and -8° SOIs are 12 and 11 CAD, respectively. The longer ignition delay with early injection is due to lower pressures and temperatures, as the mixture formation processes occur early during the compression stroke. For example, the variation of total fuel vapor mass (not shown) indicates that the peak in this value occurs near -7°CA ATDC for this case, and near TDC for the -8° SOI case. In contrast, the combustion occurs earlier or near TDC (CA50=-1.5°ATDC) for this case, and later during expansion stroke (CA50=6°ATDC) for the -8° SOI case. This leads to higher pressure and HRR for the early injection case. Consequently, the computed work, MEP, and power are also higher with early injection, for which these values are 184J, 2703.7kPa,

and 16.1kW, respectively, while the corresponding values for SOI=-8˚ are 151J, 2224.7kPa, and 13.3kW, respectively. Thus the power output increases with early injection.

Figure 12 presents the spray distribution and temperature contours for the 50% iso-octane case with SOI=-15° ATDC. The corresponding plots for SOI=-8° ATDC have been discussed earlier in the context of Figs. 8 and 9. As expected, the injection timing has strong effect on the spray, combustion, and emission characteristics. With early injection, the liquid penetration and spray formation occur in relatively lower pressure and temperature environment. This leads to greater liquid penetration with smaller lateral dispersion, and larger droplet sizes. The ignition delay is also longer with early injection, as noted earlier. In contrast, the combustion occurs near TDC for this case, and during expansion stroke for the late injection case. This leads to higher pressures and heat release rates for the early injection case, as discussed earlier (cf. Fig. 11).

The greater liquid penetration with early injection leads to increased stratification in ϕ, although the effect is partially compensated by enhanced mixing due to increased spray impingement on the piston bowl. Consequently, the ϕ distributions are not noticeably different for the two SOIs, *as illustrated[2] in Fig. 13,* which plots the temperature, ϕ, NOx and soot contours at 3° ATDC for SOI=-15°, and at 9° ATDC for SOI=-8°. Consequently, the combustion processes also appear to be generally similar for the two cases, with distinct zones of rich premixed and diffusion burning in the piston bowl, and lean premixed burning, through a lifted flame, in the spray region between the cylinder and piston. However, since the combustion occurs earlier (near TDC) for the early injection case (CA50= -1.5°ATDC), temperatures are higher, and thus NOx production is higher for this case compared to the late injection case. This is indicated more clearly in Fig. 14, which plots the volume integrated NOx and soot mass with respect to crank angle. The soot production is also higher with early injection, since a relatively larger amount of fuel ends up in the piston bowl region for this case, as illustrated in Fig. 13. Note, however, that the soot values for the two cases become nearly the same later during the expansion stroke, implying increased soot oxidation for the early injection case. Finally, the normalized soot and NOx emissions (g/kW·h) based on engine power are 0.82×10^{-5} and 7.53×10^{-5} with the early injection, and 1.03×10^{-5} and 5.0×10^{-5} with the late injection. These values correspond to the exhaust valve opening crank angle of

[2]Different crank angles have been used to account for the difference in combustion phasing for the two cases.

116^0. This implies a tradeoff between NOx and soot emissions with regards to the effect of SOI.

CONCLUSIONS

In the present study, we have examined the potential of simultaneously reducing NOx and soot emissions in CI engines by controlling the fuel reactivity and injection parameters. The fuel reactivity was varied by using a blend of n-heptane and iso-octane, which are considered as surrogate fuels for diesel and gasoline, respectively. A reduced kinetic model for the fuel blend was developed by combining the oxidation models for these two fuels, and validated against shock tube ignition data at engine relevant conditions. The combined mechanism was implemented in the commercial CFD code, CONVERGE, and engine simulations were performed to characterize the effects of blend composition and injection timing on the spray, ignition, combustion, and emission processes in a single-cylinder of a light-duty diesel engine. Important observations are as follow:

1. As a consequence of the piston bowl geometry used in this engine, the fuel consumption and heat release occur in two separate regions, one in the piston bowl and other in the spray region between the piston and cylinder. Combustion involves both the rich premixed burning and diffusion burning in the first region, and lean premixed burning in the second region. While there are distinct zones of rich premixed and diffusion burning in the piston bowl region, the combustion process does not follow the conventional Dec's model, characterized by a lifted flame with a rich premixed burning zone enveloped by a diffusion burning zone. The amounts of soot and NOx produced are determined by the relative amounts of rich premixed burning and diffusion burning, local temperatures, and combustion phasing. Furthermore, the soot and NOx formation regions correspond, respectively, to the rich premixed burning and diffusion burning zones, with the amount of NOx strongly influenced by local temperatures.
2. The spray atomization and vaporization processes are minimally affected by fuel reactivity. However, the ignition, combustion and emission processes are strongly influenced by the amount of iso-octane in the fuel blend. For a given SOI, as the fuel reactivity is reduced, the ignition delay becomes longer, and, consequently, the combustion phasing is retarded. The longer ignition delay provides additional time for fuel-air mixing, and reduces equivalence ratio stratification. Consequently, the amount of premixed combustion is enhanced relative to diffusion combustion, and, therefore, the

soot emission is reduced. The NOx emission is also reduced as a result of lower fuel reactivity, and can be attributed to two factors. First, the amount of diffusion burning is reduced relative to rich premixed burning, and second, the peak temperatures are reduced since combustion occurs further into the expansion stroke due to delayed combustion phasing.

3. The injection timing has a strong influence on the atomization and mixture formation processes, and, consequently, on the combustion and emission characteristics. With sufficiently early injection, the spray formation processes occur in relatively lower pressure and temperature environment, resulting in greater liquid penetration with smaller lateral dispersion, and longer ignition delay. However, the combustion occurs near TDC for the early injection case, and during expansion stroke for the late injection case. This leads to higher pressures and heat release rates for the early injection case. Consequently, the peak temperature and NOx emission are also higher for this case. However, the soot emission is lower for this case due to less equivalence ratio stratification. Thus, as the SOI is delayed, a tradeoff between NOx and soot emissions is observed. For instance, delaying the SOI from -15° to -8°ATDC, the normalized NOx emission (g/kW·h) decreases from 7.53×10^{-5} to 5.0×10^{-5}, while the normalized soot emission increases from 0.82×10^{-5} to 1.03×10^{-5}.
4. The present results demonstrate the potential of simultaneously reducing NOx and soot emissions in CI engines by using an appropriate blend of more reactive and less reactive fuels, and by controlling the injection parameters. While the blend reactivity strongly influences the ignition and combustion processes, the SOI affects the atomization and spray formation processes. Thus, the ignition delay and combustion phasing seem to be well correlated with fuel reactivity, while the SOI strongly affects combustion phasing.
5. Simulations also indicate an operability range in terms of the blend composition and SOI beyond which the fuel-air mixture may not be sufficiently well mixed, or compression ignited. For instance, for a given SOI, the mixture would fail to ignite if the amount of less reactive fuel exceeds a certain limit. Similarly, for a given blend composition, the mixture may not ignite if the SOI is delayed beyond a certain value. Nevertheless, the study underline the possibility of designing an optimum parametric space in terms of blend composition, SOI, and other variables in order to significantly reduce engine emissions for a given load and speed. Hence, CI engines employing a blended fuel strategy can achieve low emissions and high thermal efficiency, but without additional equipment, such as a second injection or a mixing manifold, used in other strategies.

ACKNOWLEGEMENT

This work was partially supported by the U.S. Department of Energy Office of Vehicle Technology (ANL Contract # 6F-00004) under the management of Mr. Gurpreet Singh. Dr. Stephen Ciatti was the technical monitor. Many of the simulations were performed by Hwansoo Chong, when he was a graduate student at UIC. Authors greatly appreciate the extensive technical assistance provided by Dr. P. K. Senecal of Convergent Science in running the CFD code.

List of Tables

List of Figures

Figure 5. Pressure and heat release rate profiles with respect to crank angle for three grid sizes.

Figure 6. Computed pressure and heat release rate profiles with respect to crank angle for with three different n-heptane/iso-octane blends and SOI=-8°CA ATDC. Blends include 100%-n-heptane, 90%-n-heptane/10%-iso-octane, and 50%-n-heptane/50%-iso-octane by volume.

Figure 7. Total NOx and soot formed in the cylinder versus CAD for three different blends as discussed in the context of Fig. 6.

Figure 8. Spray distribution at CA of -7˚, -3˚, -1˚, and 0˚ ATDC for pure n-heptane (left) and CA of -7˚, -3˚, -1˚, 0˚, 1˚, and 2˚ ATDC for 50%-iso-octane blend, SOI=-8°CA ATDC.

Figure 9. Spray distribution and temperature contour at CA of -1˚, 0˚, 1˚, 2˚, 3˚,and 4˚ ATDC for pure n-heptane (left) and CA of 2˚, 3˚, 5˚, 6˚, 7˚, and 8˚ ATDC for 50%-iso-octane blend, SOI=-8°CA ATDC.

Figure 10. Iso-temperature, equivalence ratio, NOx and soot contours plotted at 4° ATDC for the 0%-iso-octane (100% n-heptane) case, and at 7° ATDC for the 50%-iso-octane case.

Figure 11. Pressure and heat release rate profiles versus crank angle for simulations performed with 50%-iso-octane blend for three different SOIs.

Figure 12. Spray distribution (left) at CA of -14˚, -10˚, -8˚, -4˚, and -3˚ ATDC and temperature contours at CA of -3˚, -2˚, -1˚, 0˚, and 1˚ ATDC for 50%-iso-octane blend, SOI=-15° ATDC.

Figure 13. Iso-temperature, equivalence ratio (ϕ), NOx and soot contours plotted at 3° ATDC for SOI=-15° ATDC (left), and at 9° ATDC for SOI=-8° ATDC. The fuel contains 50% iso-octane. Temperature values are between 600K and 2800K, ϕ between 0.2 and 2., NOx between 0 and 0.003kg, soot between 0.0001 to 0.0013kg.

Figure 14. Volume integrated NOx and soot mass versus crank angle for two different SOIs with 50%-iso-octane blend.

Table 1. Common reactions included in both the iso-octane and n-heptane oxidation mechanisms but with different kinetic parameters.

No.	Reaction	Reaction mechanism					
		n-heptane (k_1)			iso-octane (k_2)		
		A	β	E (cal/mol)	A	β	E (cal/mol)
R1	h2o2+m⇔oh+oh+m	4.3×10^{16}	0	45500	1×10^{17}	0	45500
R2	c3h7=c2h4+ch3	9.6×10^{13}	0	30950	9.6×10^{13}	0	35900
R3	co+oh=co2+h	3.51×10^{7}	1.3	-758	5.99×10^{7}	1.3	5232.877
R4	oh+ch3o=h2o+ch2o	1×10^{13}	0	0	5×10^{12}	0	0
R5	h2o2+m=oh+oh+m	3.6×10^{17}	-0.72	0	3.6×10^{17}	-0.7	0
R6	ho2+ho2=h2o2+o2	2×10^{12}	0	0	3×10^{12}	0	0
R7	ch2o+oh=hco+h2o	2.43×10^{12}	1.2	-447	5.563×10^{10}	1.095	-76.517
R8	hco+m=h+co+m	1.87×10^{17}	-1	17000	1.591×10^{18}	0.95	56712.33
R9	ch3+ch3o=ch4+ch2o	4.1×10^{14}	0	0	4.3×10^{14}	0	0
R10	ch4+ho2=ch3+h2o2	1×10^{13}	0	18700	9×10^{11}	0	18700

Table 2. Simulation conditions

Engine speed, (RPM)	1500
Gas temperature at intake valve closing (IVC), (K)	310
Gas pressure at IVC, (bar)	1.23
IVC, (CAD)	-132 ATDC
Exhaust valve opening (EVO), (CAD)	116 ATDC
Start of injection (SOI), (CAD)	-15, -8, -0.5 ATDC
Injection Duration	8 CAD
Fuel intake temperature, (K)	298
Cylinder head temperature, (K)	500
Cylinder wall temperature, (K)	450
Piston wall temperature, (K)	550
Mass of fuel injected/injector/nozzle, (kg/cycle)	1.2495×10^{-6}
Mass fraction of iso-octane in blended fuel (%)	0, 10, 50, 90

Table 3. Base grid sizes and grid scale levels for examining grid size effects

Case number	1	2	3
Base grid size (mm)	1	2	3
Grid scale prior to injection, from -145 to 22 CAD	-1	-1	-1
Grid size prior to injection, from -145 to 22 CAD (mm)	2	4	6
Grid scale near nozzle (fixed embedding)	2	2	3
Grid size near nozzle (mm)	0.25	0.5	0.375
Grid scale near piston wall, cylinder head (fixed embedding)	1	1	2
Grid size near piston wall, cylinder head (mm)	0.5	1	1.5
AMR grid scales for velocity, temperature, species	2	2	3
AMR grid sizes (mm) for velocity, temperature, species	0.25	0.5	0.375
Approximate number of grid cells	10^6	10^5	10^4

Table 4. Physical (t_p), chemical (t_c), and total ignition delay time ($t_{ig}= t_p+ t_c$,) in terms of °CA for four different n-heptane/iso-octane blends and three different SOIs.

SOI (˚CA ATDC)	0% (pure n-heptane)			10% iso-octane			50% iso-octane			90% iso-octane		
	t_p	t_c	t_{ig}	t_p	t_c	t_{ig}	t_p	t_c	t_{ig}	t_p	t_c	t_{ig}
-15	6	3	9	6	5	11	6	6	12	No ignition		
-8	5	3	8	5	5	10	5	6	11	No ignition		
-0.5	4	4	8	No ignition			No ignition			No ignition		

Table 5. Properties of n-heptane and iso-octane.

Property	n-heptane	iso-octane
Molar weight (kg/kmol)	100.2	114.23
Density at 298 K (kg/m^3)	684	690
Boiling point (K)	371	372
LHV (kJ/kg)	44,926	44,310
Heat of vaporization (kJ/mol)	31.77	32.26
Viscosity (mPa·s)	0.42	0.5
Cetane number	56	16

Table 6. Computed work, MEP, power per cylinder, and emissions for the three blends with SOI=-8˚ ATDC.

Blend composition by volume (%)		Engine performance			Emissions (g/kW·h)	
n-heptane	Iso-octane	Work (J)	MEP (kPa)	Power (kW)	NOx	Soot
100	0	166	2445.5	14.6	7.4×10^{-5}	1.5×10^{-5}
90	10	161	2372.3	14.2	4.7×10^{-5}	1.7×10^{-5}
50	50	151	2224.7	13.3	5.0×10^{-5}	1.1×10^{-5}

(a): n-heptane/air

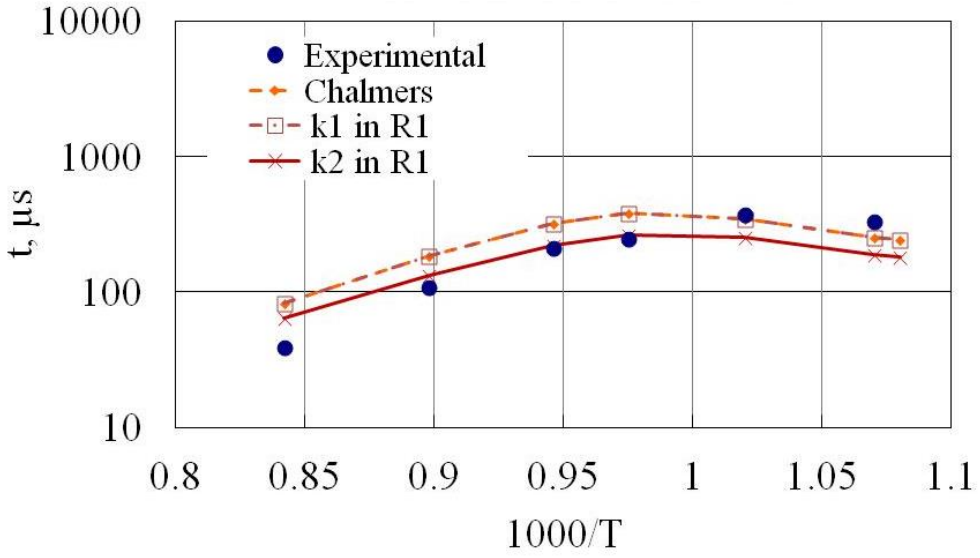

(b): iso-octane/air

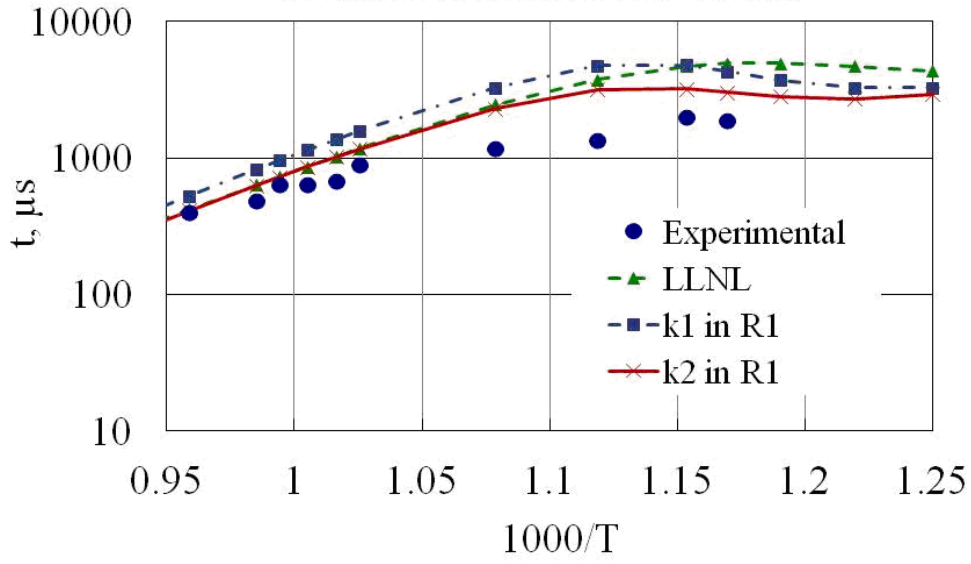

Figure 1. Comparison of ignition delay predictions with measurements of Gauthier et al. (2004) for n-heptane/air mixture (Fig. 1a), and those of Davidson et al. (2005) for iso-octane/air mixture at p=55 atm and ϕ=1. Ignition delays predicted using the detailed LLNL mechanism are shown in Fig. 1b.

(a)

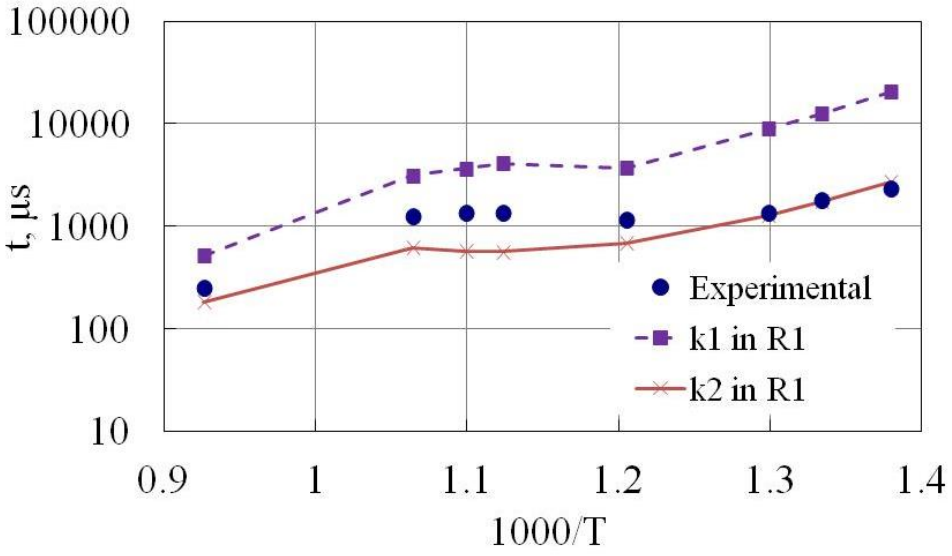

(b)

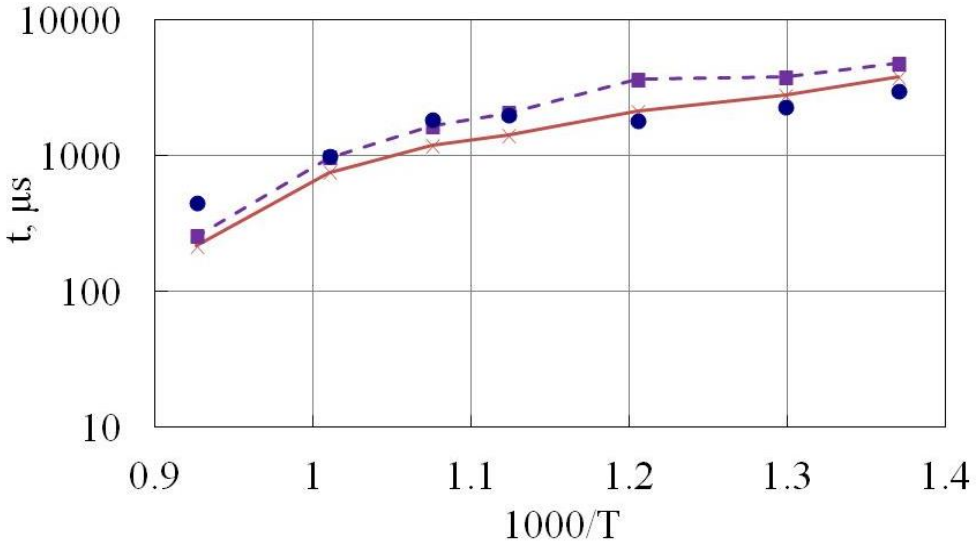

Figure 2. Comparison of ignition delay predictions with measurements of Fieweger et al. (1997) for n-heptane/iso-octane/air mixtures at p=40 atm and ϕ=1. Results are shown for two blends with 60% iso-octane by volume in Fig. 2a, and 80% iso-octane in Fig. 2b.

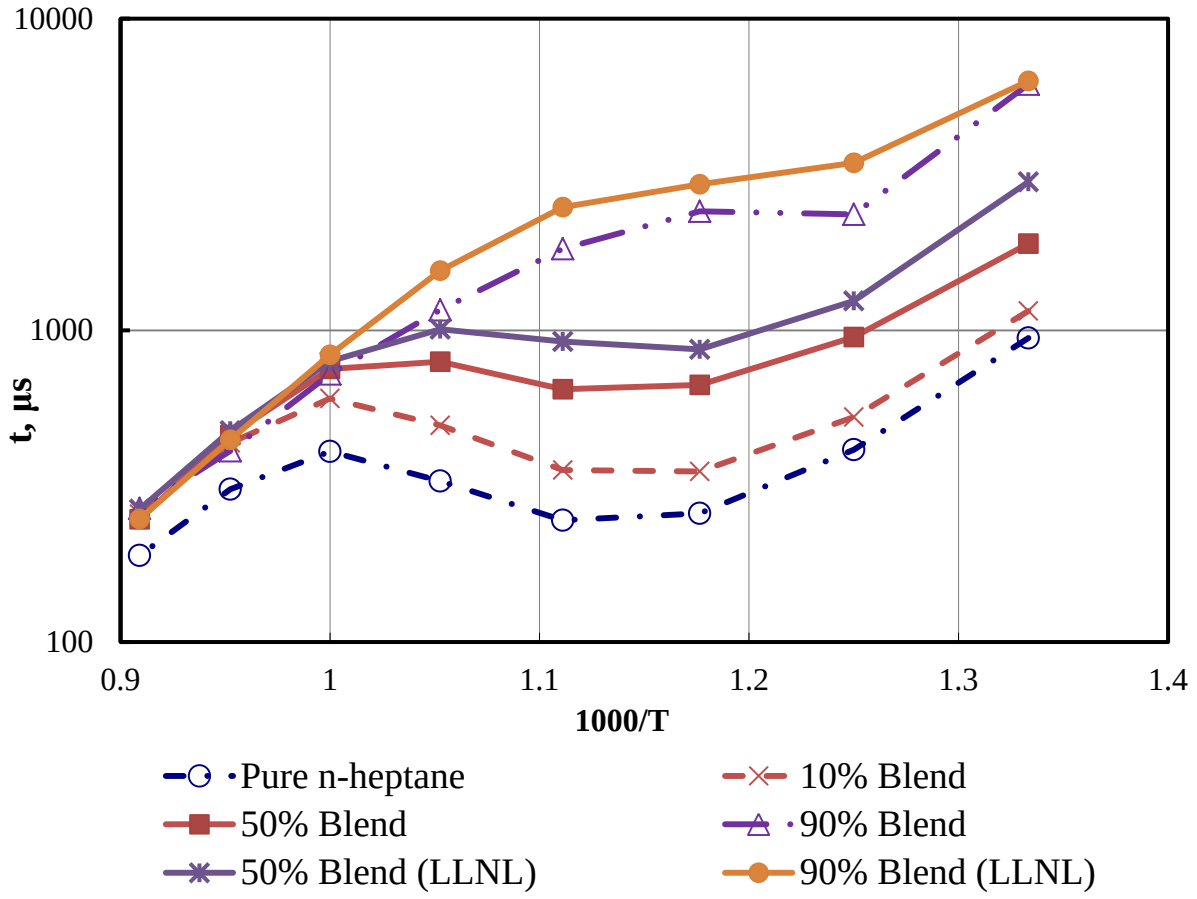

Figure 3. Predicted ignition delays versus inverse of temperature for n-heptane/iso-octane blends containing with 0, 10%, 50%, and 90% iso-octane by volume, and at p=45 atm, and ϕ=1. Predictions using the LLNL mechanism for 50%- and 90%-iso-octane blends are also shown.

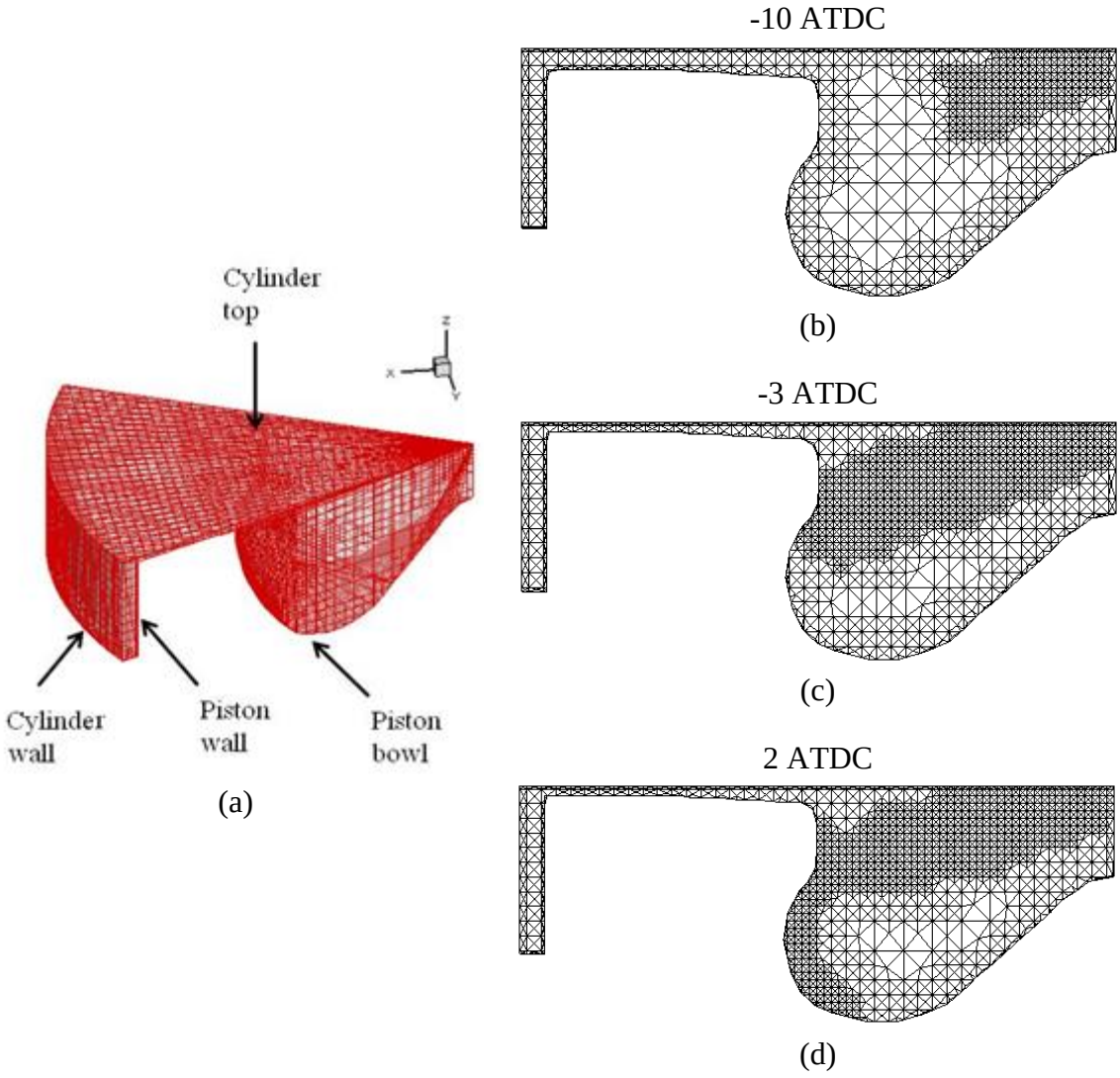

Figure 4. Computational grid and 1/7 sector for 1.9L 4-cylinder GM light-duty diesel engine with a 7-hole common-rail injector (a). Figures (b), (c), (d) show the cut plane view of the computational grid through the center of the nozzle at CA of -10°, -3° and 2° ATDC (for 50%-iso-octane blend, SOI=-8° ATDC), and demonstrate the capability of adaptive grid refinement to resolve the flow field near the spray.

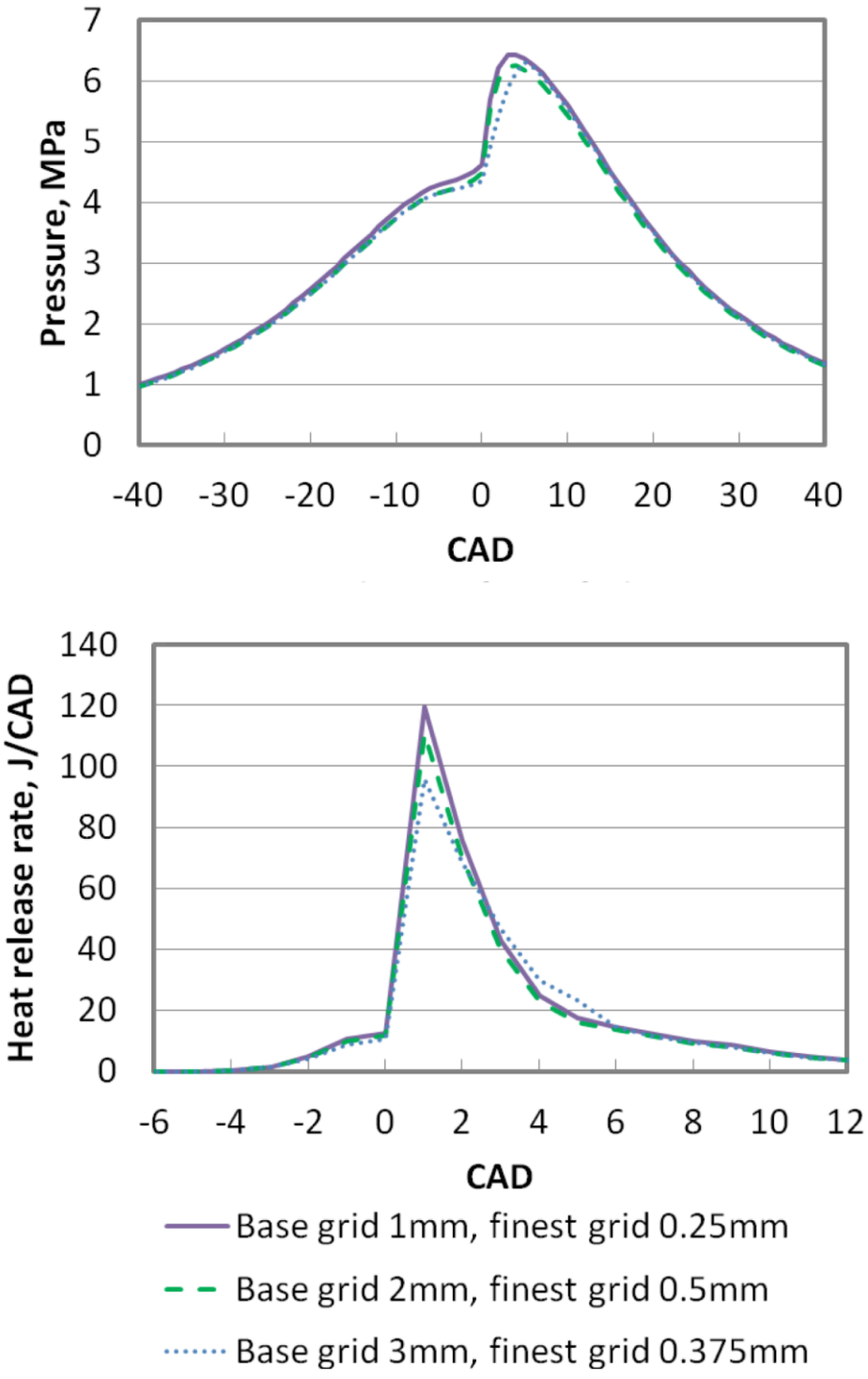

Figure 5. Pressure and heat release rate profiles with respect to crank angle for three grid sizes.

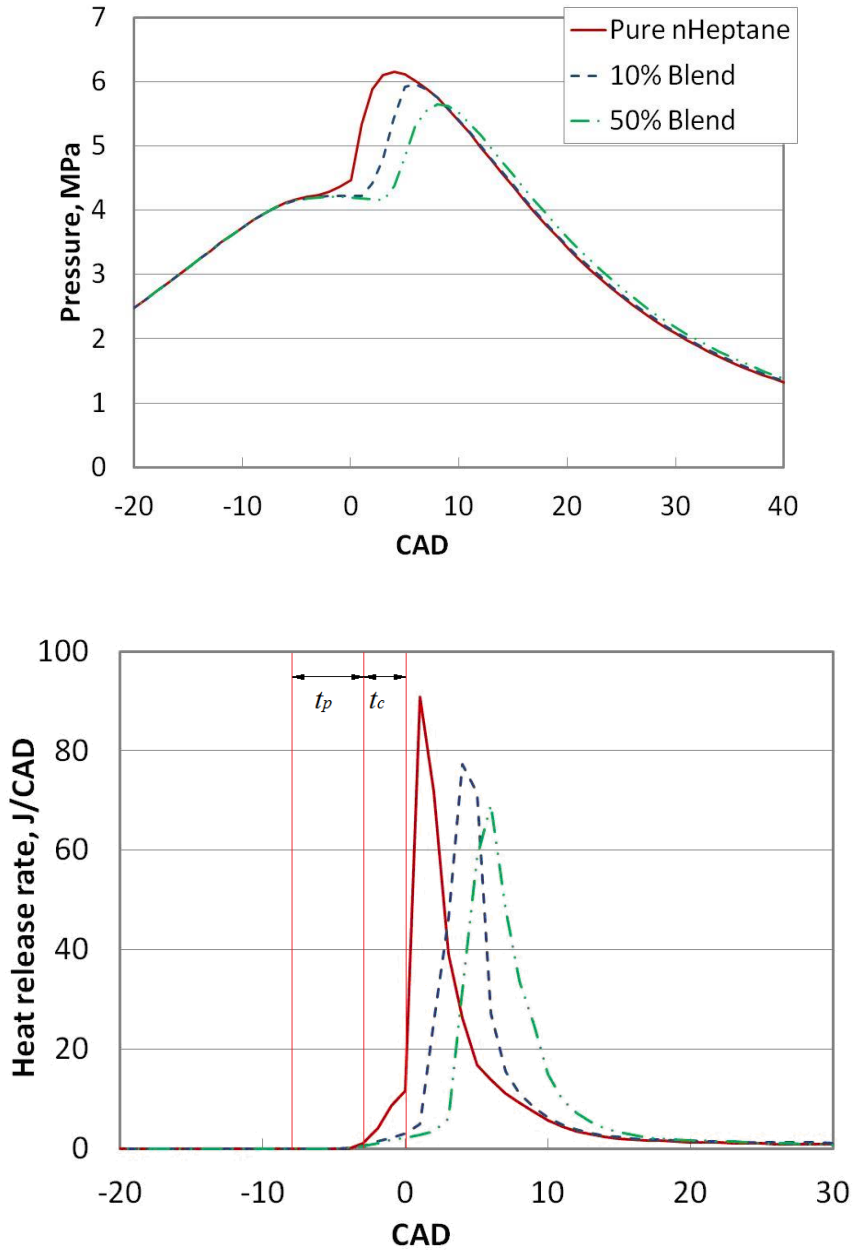

Figure 6. Computed pressure and heat release rate profiles with respect to crank angle for three different n-heptane/iso-octane blends and with SOI=-8°CA ATDC. Blends include 100%-n-heptane, 90%-n-heptane/10%-iso-octane, and 50%-n-heptane/50%-iso-octane by volume. Vertical lines indicate the physical delay (t_p) and chemical delay (t_c) for the 100% n-heptane case.

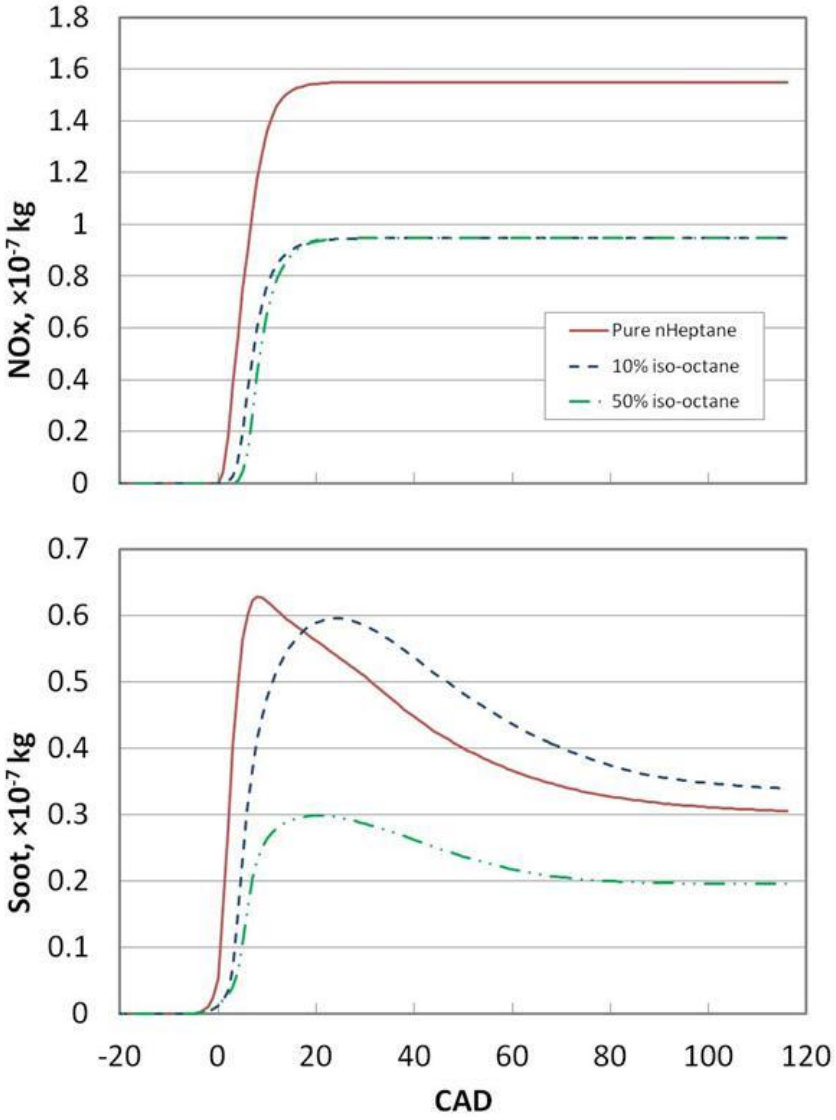

Figure 7. Total NOx and soot formed in the cylinder versus CAD for three different blends as discussed in the context of Fig. 6.

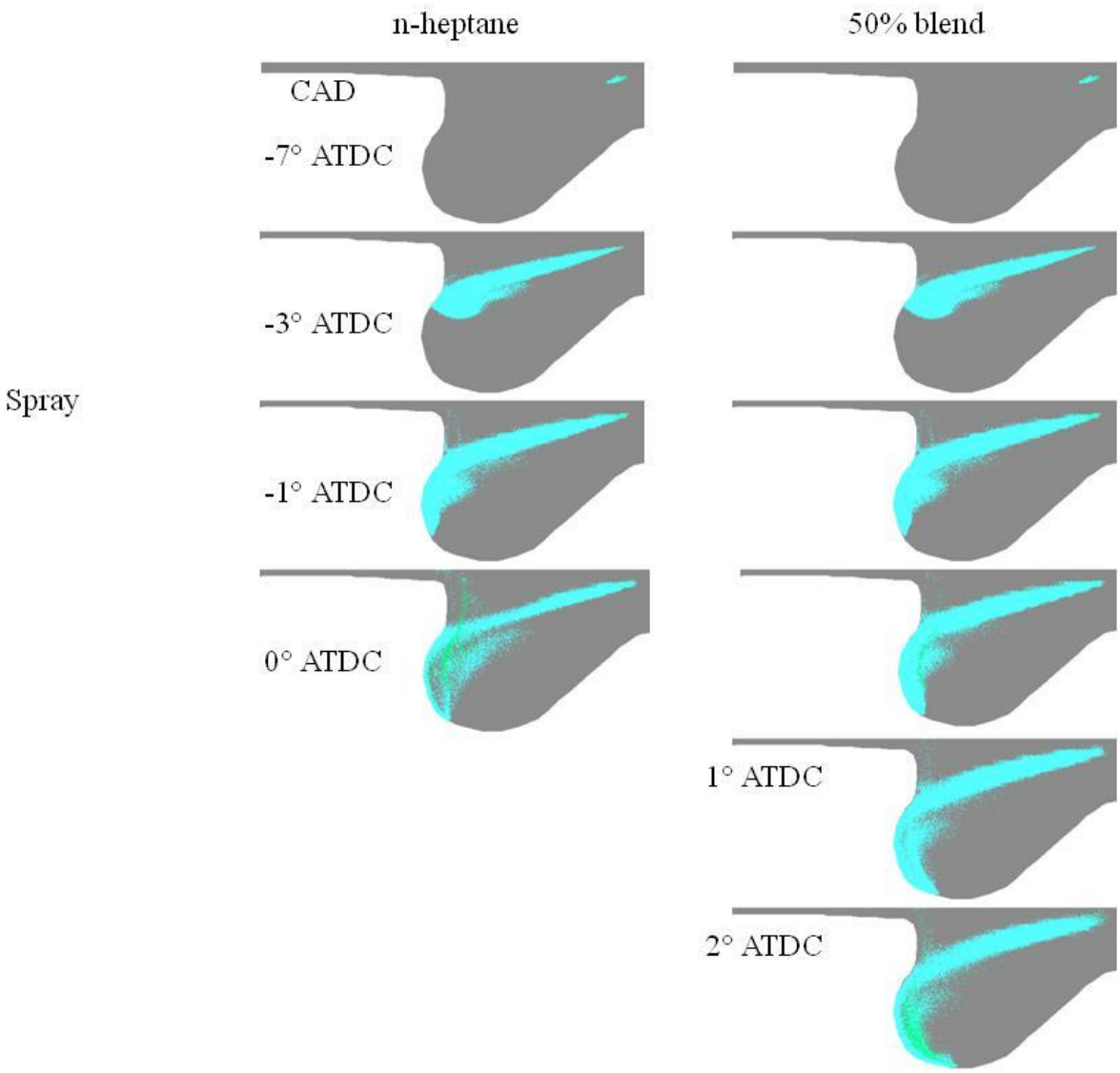

Figure 8. Spray distribution at CA of -7˚, -3˚, -1˚, and 0˚ ATDC for pure n-heptane (left) and CA of -7˚, -3˚, -1˚, 0˚, 1˚, and 2˚ ATDC for 50%-iso-octane blend, SOI=-8°CA ATDC.

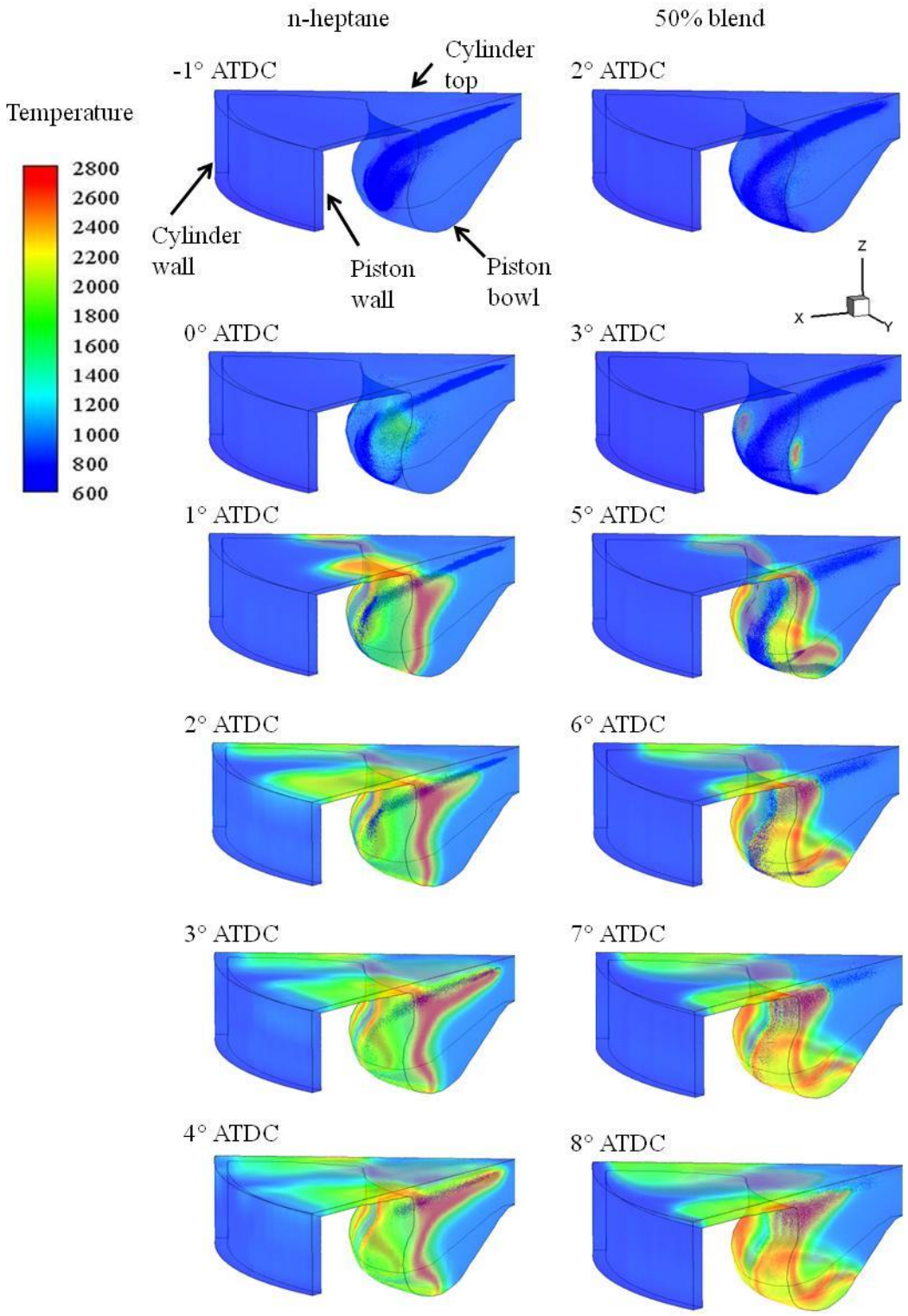

Figure 9. Spray distribution and temperature contour at CA of -1˚, 0˚, 1˚, 2˚, 3˚,and 4˚ ATDC for pure n-heptane (left) and CA of 2˚, 3˚, 5˚, 6˚, 7˚, and 8˚ ATDC for 50%-iso-octane blend, SOI=-8°CA ATDC.

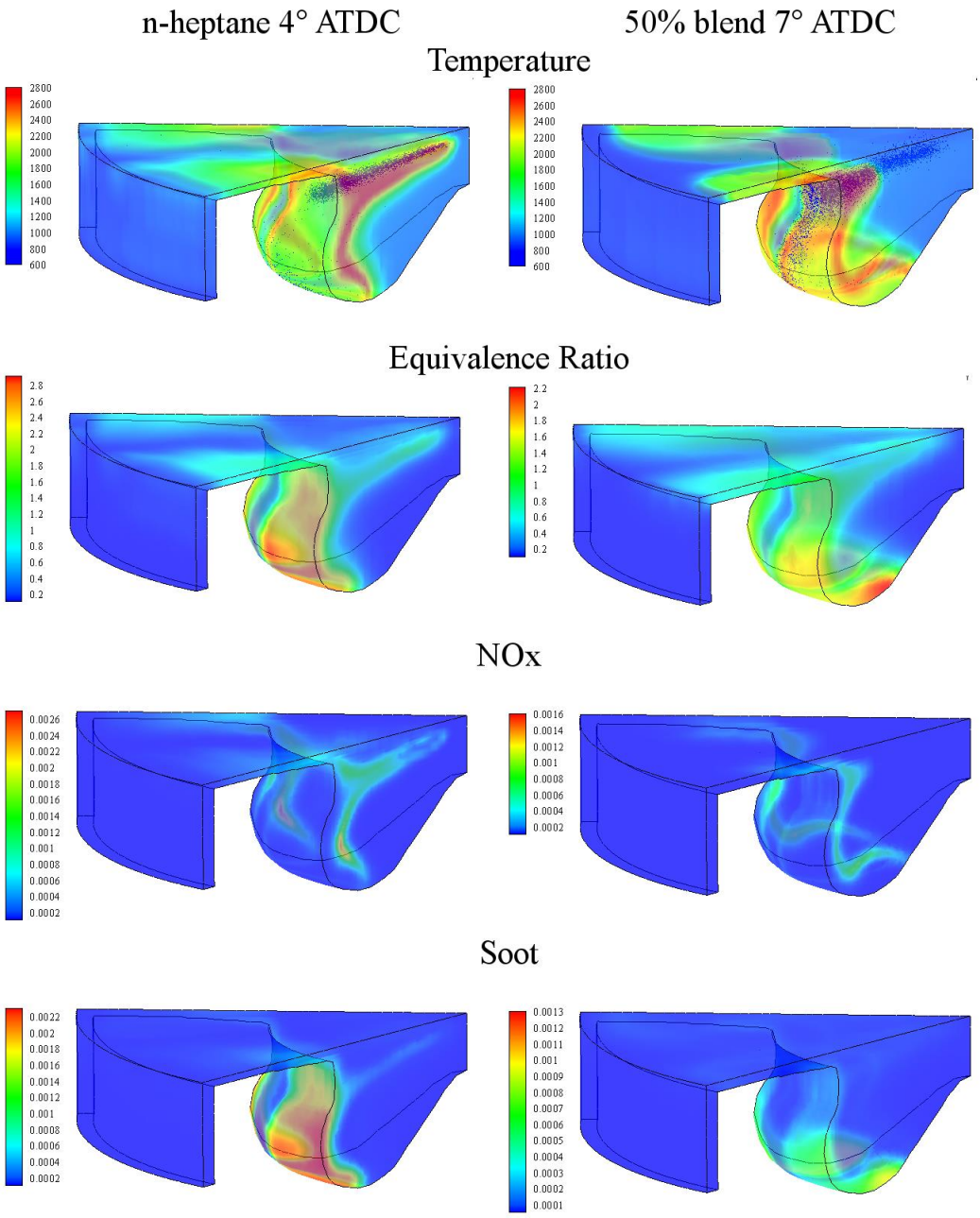

Figure 10. Iso-temperature, equivalence ratio, NOx and soot contours plotted at 4° ATDC for the 0%-iso-octane (100% n-heptane) case, and at 7° ATDC for the 50%-iso-octane case.

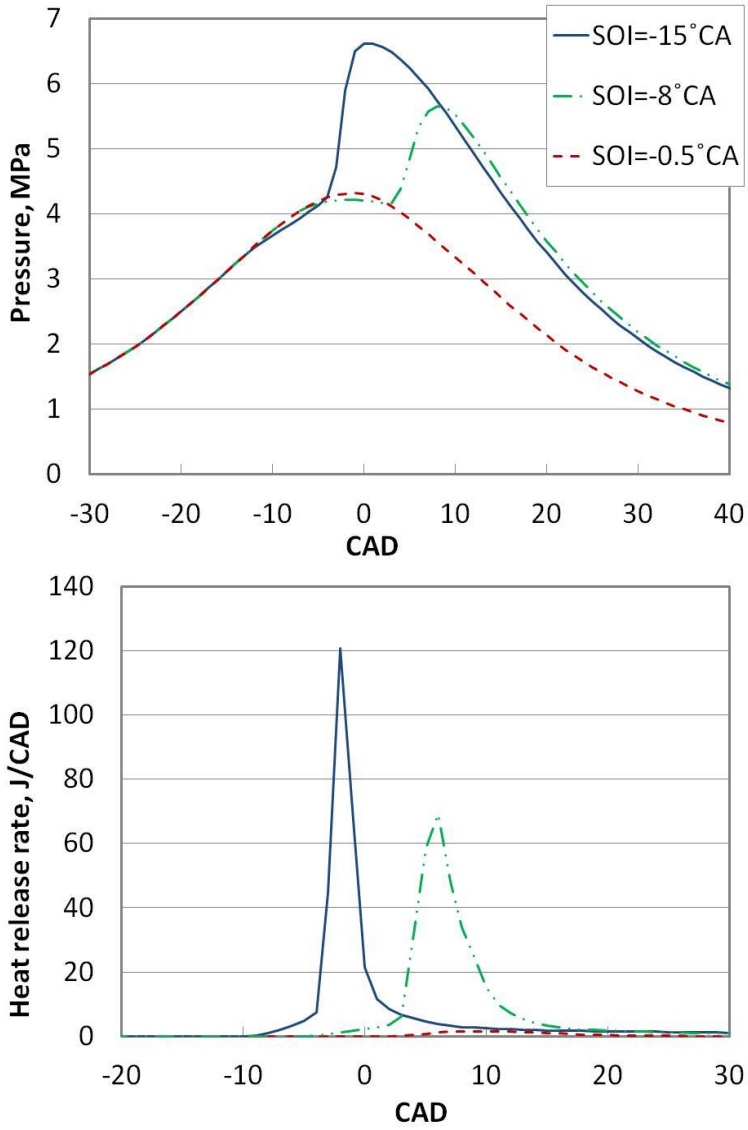

Figure 11. Pressure and heat release rate profiles versus crank angle for simulations performed with 50%-iso-octane blend for three different SOIs.

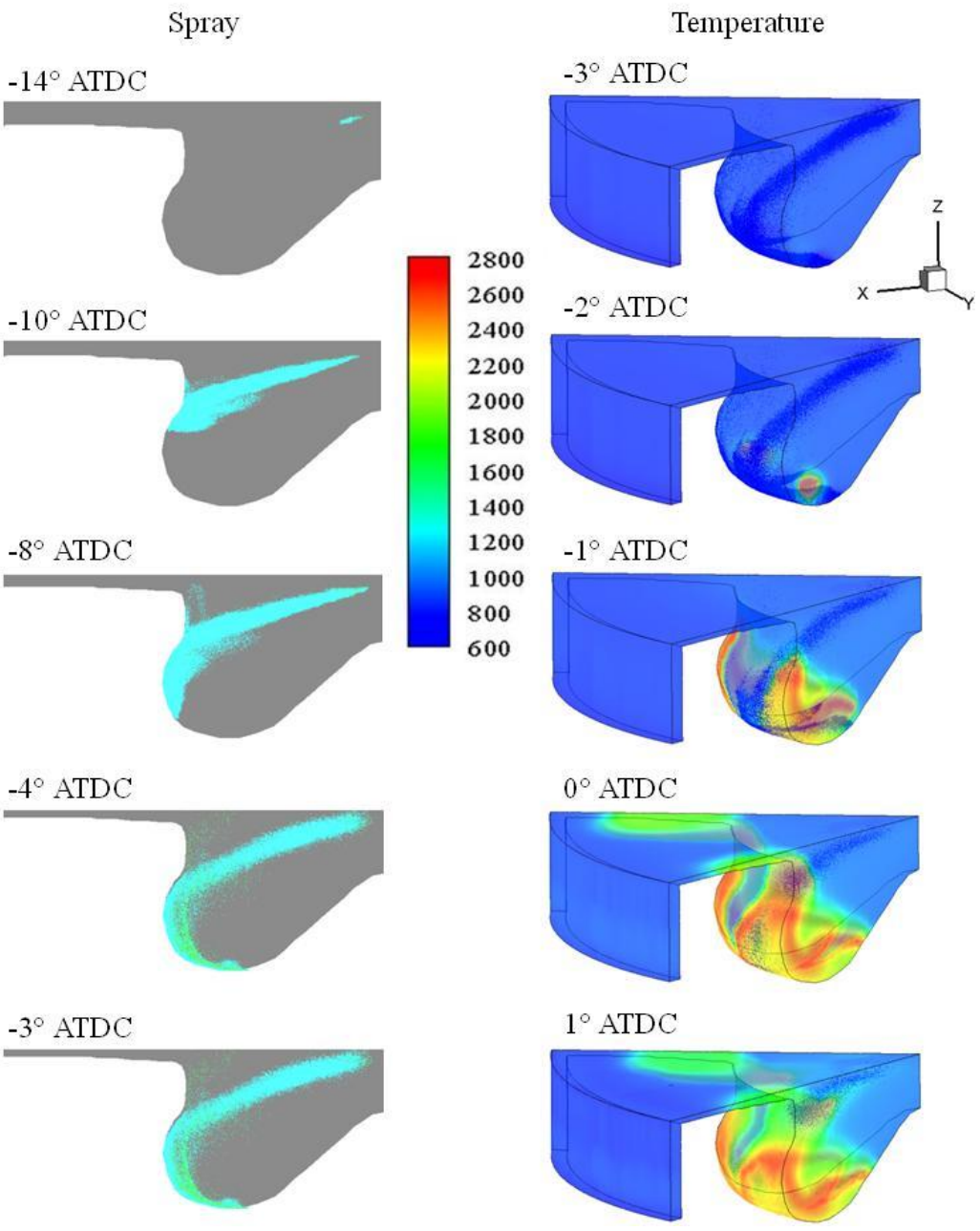

Figure 12. Spray distribution (left) at CA of -14˚, -10˚, -8˚, -4˚, and -3˚ ATDC and temperature contours at CA of -3˚, -2˚, -1˚, 0˚, and 1˚ ATDC for 50%-iso-octane blend, SOI=-15° ATDC.

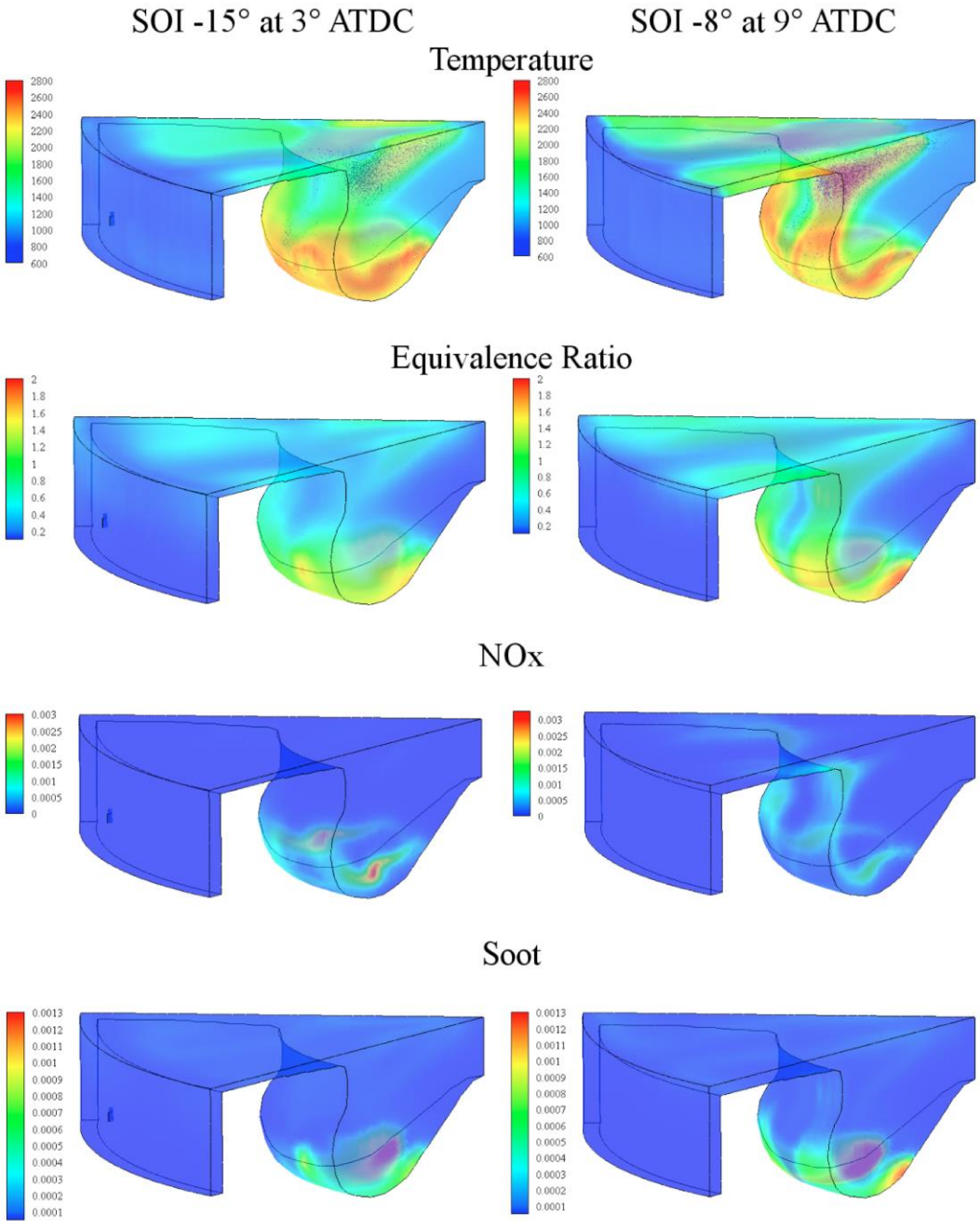

Figure 13. Iso-temperature, equivalence ratio (ϕ), NOx and soot contours plotted at 3° ATDC for SOI=-15° ATDC (left), and at 9° ATDC for SOI=-8° ATDC. The fuel contains 50% iso-octane. Temperature values are between 600K and 2800K, ϕ between 0.2 and 2, NOx between 0 and 0.003kg, soot between 0.0001 to 0.0013kg.

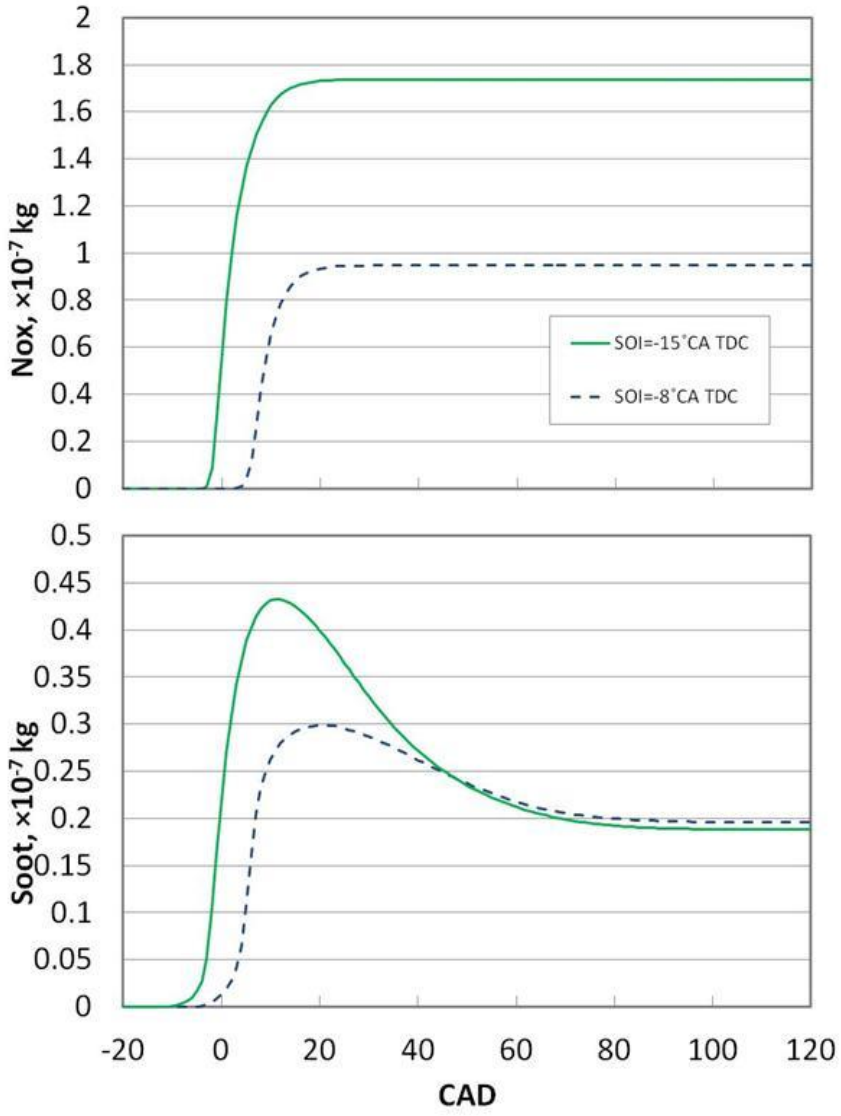

Figure 14. Volume integrated NOx and soot mass versus crank angle for two different SOIs with 50%-iso-octane blend.

References

Tanaka S, Ayala F, Keck JC, Heywwod JB, (2003). 'Two-stage ignition in HCCI combustion and HCCI control by fuels and additives', *Combustion and Flame,* Vol. 132 No. 1-2, pp. 219-239.

Kong SC, Reitz RD, (2002). 'Use of detailed chemical kinetics to study HCCI engine combustion with consideration of turbulent mixing effects', *Journal of Engineering for Gas Turbines and Power,* Vol. 124 No. 3, pp. 702-707.

Dec JE, (2009). 'Advanced compression-ignition engines-understanding the in-cylinder processes', *Proceedings of the Combustion Institute*, Vol. 32, pp. 2727-2742.

Mueller CJ, Martin GC, Briggs TE, Duffy KP, (2004). 'An experimental investigation of in-cylinder processes under dual-injection conditions in a DI diesel engine', S*AE Paper* 2004-01-1843.

Kimura S, Aoki SO, Kitahara Y, Aiyoshizawa E, (2001). 'Ultra-clean combustion technology combining a low-temperature and premixed combustion concept for meeting future emission standards', *SAE Paper* 2001-01-0200.

Diwakar R, Singh S, (2008). 'NOx and soot reduction in diesel engine premixed charge compression ignition combustion: a computational investigation', *International Journal of Engine Research,* Vol. 9. No. 3, pp. 195-214.

Reitz RD, (2012). 'Directions in internal combustion engine research', *Combustion and Flame,* Vol. 160, pp. 1-8.

Wang D, Zhang C, Wang Y (2007). 'A Numerical Study of Multiple Fuel Injection Strategies for NOx Reduction from DI Diesel Engines', *International Journal of Green Energy,* Vol. 4, No. 4, pp. 453-470.

Ni P, Wang X, (2012). 'Modeling the Formation of Nox and Soot Emissions in a Diesel Engine at Different Humidity', *International Journal of Green Energy,* Vol. 9, No. 8, pp. 815-828.

Brijesh P, Chowdhury A, Sreedhara S, (2014). 'Simultaneous reduction of NOx and PM using ultra-cooled EGR and retarded injection timing in a diesel engine', *International Journal of Green Energy,* DOI:10.1080/15435075.2013.841164.

Korakianitis T, Namasivayam AM, Crookes RJ, (2011). 'Natural-gas fueled spark-ignition (SI) and compression-ignition (CI) engine performance and emissions', *Progress in Energy and Combustion Science,* Vol. 37, pp. 89-112.

Gray AW, Ryan TW, (1997). 'Homogeneous charge compression ignition of diesel fuel', *SAE Paper* 1997-971676.

Christensen M, Hultqvist A, Johansson B, (1999). 'Demonstrating the multi-fuel capability of a homogeneous charge compression ignition engine with variable compression ratio', *SAE Paper* 1999-01-3679.

Kaahaaina NB, Simon AJ, Caton PA, Edwards CF, (2001). 'Use of dynamic valving to achieve residual-affected combustion', *SAE Paper* 2001-01-0549.

Lee CH, Lee KH, (2007). 'An experimental study on the combustion and emission characteristics of a stratified charge compression ignition (SCCI) engine', *Energy & Fuel*, Vol. 21, pp.1901-1907.

Kalghatgi GT, Risberg P, Ångström HE, (2006). 'Advantages of fuels with high resistance to auto-ignition in late injection, low-temperature, compression ignition combustion', *SAE Paper* 2006-01-3385.

Kalghatgi GT, Hildingsson L, Harrison AJ, Johansson B, (2011). 'Autoignition quality of gasoline fuels in partially premixed combustion in diesel engines', *Proceedings of the Combustion Institute*, Vol. 33, pp. 3015-3021.

Changwei J, Shuofeng W, (2009). 'Effect of hydrogen addition on the idle performance of a spark ignited gasoline engine at stoichiometric condition', *International Journal of Hydrogen Energy*, Vol. 34, pp. 3546-56.

Bayraktar H, (2005). 'Experimental and theoretical investigation of using gasoline-ethanol blends in spark-ignition engines', *Renewable Energy*, Vol. 30, No. 11, pp. 1733-1747.

Irimescu A, (2012). 'Performance and fuel conversion efficiency of a spark ignition engine fueled with iso-butanol. *Applied Energy*, Vol. 96, pp. 477-483.

Saravanan N, Nagarajan G, Narayanasamy S, (2008). 'An experimental investigation on DI diesel engine with hydrogen fuel', *Renewable Energy*, Vol. 33, No. 3, pp. 415-421.

Karabektas M, Hosoz M, (2009). 'Performance and emission characteristics of a diesel engine using isobutanol-diesel fuel blends', *Renewable Energy*, Vol. 34, No. 6, pp. 1554-1559.

Lapuerta M, Armas O, Rodríguez-Fernández J, (2008). 'Effect of biodiesel fuels on diesel engine emissions', *Progress in Energy and Combustion Science*, Vol. 34, No. 2, pp. 198-223.

Alam M, Song J, Zello V, Boehman A, (2004). 'Spray and combustion visualization of a direct-injection diesel engine operated with oxygenated fuel blends', *International Journal of Engine Research*, Vol. 7, pp. 503-521.

Peng Z, Zhao H, Ladommatos N, (2003). 'Visualization of the homogeneous charge compression ignition/controlled autoignition combustion process using two-dimensional planar laser-induced fluorescence imaging of formaldehyde', *Proceedings of the Institution of Mechanical Engineers, Part D: Journal of Automobile Engineering*, Vol. 217, pp. 1125-1134.

Dumitrescu CE, Guo H, Hosseini V, Neill WS, Chippior WL, Connolly T, Graham L, Li H, (2011). 'The effect of iso-octane addition on combustion and emission characteristics of a HCCI engine fueled with n-heptane', *Journal of Engineering for Gas Turbines and Power*, Vol. 133, 112801-1-7.

Lu X.C., Chen W, Huang Z, (2005). 'A fundamental study on the control of the HCCI combustion and emissions by fuel design concept combined with controllable EGR Part 1. The basic characteristics of HCCI combustion', *Fuel*, Vol. 84, pp. 1074-1083.

Shahbakhti M, Koch CR, (2008). 'Characterizing the cyclic variability of ignition timing in a homogeneous charge compression ignition engine fuelled with n-heptane/iso-octane blend fuels', *International Journal of Engine Research*, Vol. 9, pp. 361-397.

Hu Z, Cracknell RF, Somers LMT, (2011). 'Computational study of fuel effects in premixed charge compression ignition (PCCI) engine combustion', *Proceedings of European Combustion Meeting,* 2011.

Kokjohn SL, Reitz RD, (2009). 'A modeling study of charge preparation and combustion in an HCCI engine using a variable pressure pulse (VPP) injection system and optimized PRF blends', *Proceedings of DEER Conference* 2009.

López JJ, Novella R, García A, Winklinger JF, (2013). 'Investigation of the ignition and combustion processes of a dual-fuel spray under diesel-like conditions using computational fluid dynamics (CFD) modeling', *Mathematical and Computer Modeling,* Vol. 57, pp. 1897-1906.

Richards KJ, Senecal PK, Pomraning E, (2012). *CONVERGE (Version 1.4.1), Convergent Science, Inc.,* Middleton, WI.

Som S, Aggarwal SK, (2010). 'Effects of primary breakup modeling on spray and combustion characteristics of compression ignition engines', *Combustion and Flame,* Vol. 157, pp. 1179-1193.

Aggarwal SK, Longman DE, (2011). 'A computational study on the effects of pre-ignition processes on diesel engine combustion and emissions', *Proceedings of ASME/JSME 8th Thermal Engineering Joint Conference*. AJTEC 2011-44202

Reitz RD, Diwakar R, (1987). 'Structure of high pressure sprays', *SAE Trans* 1987;96:492-509.

Patterson MA, Reitz RD, (1998). 'Modeling the effects of fuel spray characteristics on diesel engine combustion and emission', *SAE Paper* 1998-980131.

Schmidt DP, Rutland CJ, (2000). 'A new droplet collision algorithm', *Journal of Computational Physics,* Vol. 164, pp. 62-80.

Poster SL, Abraham J, (2002). 'Modeling collision and coalescence in diesel spray', *International Journal of Multiphase Flow,* Vol. 28, pp. 997-1019.

Chiang CH, Raju MS, Sirignano WA, (1992). 'Numerical analysis of a convecting, vaporizing fuel droplet with variable properties', *International Journal of Heat and Mass Transfer,* Vol. 35, pp. 1307.

Liu AB, Mather DK, Reitz RD, (1993). 'Modeling the effects of drop drag and breakup on fuel sprays', *SAE Paper* 1993-93007.

Senecal PK, Pomraning E, Richards KJ, (2003). 'Multi-dimensional modeling of direct-injection diesel spray liquid length and flame lift-off length using CFD and parallel detailed chemistry', *SAE Paper*. 2003-01-0243.

Dr. Valeri Golovichev's Home Page : *http://www.tfd.chalmers.se/~valeri/MECH.html*.

Jia M, Xie M. (2006). 'A chemical kinetics model of iso-octane oxidation for HCCI engines', *Fuel,* Vol. 85, pp. 2593-2604.

CHEMKIN 10101, Reaction Design: San Diego, (2010).

Gauthier BM, Davidson DF, Hanson RK, (2004). 'Shock tube determination of ignition delay times in full-blend and surrogate fuel mixtures', *Combustion and Flame,* Vol. 139, pp. 300-311.

Davidson DF, Gauthier BM, Hanson RK., (2005). 'Shock tube ignition measurements of iso-octane/air and toluene/air at high pressures'. *Proceedings of the Combustion Institute,* Vol. 30, pp. 1175-1182.

LLNL (2013) *https://www-pls.llnl.gov/data/docs/science_and_technology/chemistry/combustion/ic8_ver3_mech.txt.*

Fieweger K, Bluementhal R, Adomeit G, (1997). 'Self ignition of SI engine model fuels: A shock tube investigation at high pressure', *Combustion and Flame,* Vol. 109, pp. 599-619.

Siebers DL, Higgins B, (2001). 'Flame lift-Off on direct-injection diesel sprays under quiescent conditions', *SAE Paper* 2001-01-0530.

Higgins B, Siebers DL, (2001). 'Measurement of the flame lift-off location on DI diesel sprays using OH chemiluminescence', *SAE Paper* 2001-01-0918.

Aggarwal SK, (1998). 'A Review of Spray Ignition Phenomenon: Present Status and Future Research', *Progress in Energy and Combustion Science,* Vol. 24, No. 6, pp. 565-600.

Flynn PF, Durrett RP, Hunter GL, Loye AO, Akinyemi OC, Dec JE, Westbrook CK, (1999). 'Diesel combustion: An integrated view combining laser diagnostics, chemical kinetics, and empirical validation', *SAE Paper* 1999-01-0509.